Geochemical and Geophysical Evaluation of Structural Pathways Controlling Metallic Mineralization in the Okemesi Fold Belt, Southwestern Nigeria

Ayodele Samuel Olusiji[1], Olususi Joseph Ige[2], *Adebisi Matthew Iwabi[3]

[1]Department of Applied Geology, the Federal University of Technology, Akure, Ondo State, Nigeria

[2]Nigerian Geological Survey Agency, Akure, Ondo State, Nigeria

[3]Department of Applied Geology, the Federal University of Technology, Akure, Ondo State, Nigeria

***Corresponding Author**

DOI: https://doi.org/10.51584/IJRIAS.2026.11060127

Received: 13 June 2026; Accepted: 18 June 2026; Published: 01 July 2026

ABSTRACT

The Okemesi Fold Belt, located within the southwestern Nigerian Basement Complex, is a structurally complex Pan-African terrain with documented occurrences of gold and base-metal mineralization. However, systematic evaluation of its structural and lithological controls remains limited. This study applies an integrated geological, petrographic, geophysical, radiometric, and geochemical approach to delineate structurally controlled mineralized zones and develop a mineral systems framework. Airborne aeromagnetic and radiometric datasets from the 2009 Fugro survey were processed using reduction to the equator, regional–residual separation, analytical signal enhancement, lineament extraction, and Euler deconvolution to map lithological boundaries, faults, and shear zones. Radiometric data for K, Th, and U were analyzed to identify hydrothermal alteration and lithological variations. These datasets were integrated with 1:25,000-scale geological mapping, petrographic analysis of representative lithologies, and multi-element geochemical analyses of thirty-six rock samples, including migmatites, banded gneisses, schists, quartzites, pegmatites, and charnockites. Multivariate statistical analyses highlighted significant elemental associations and anomalous zones. Results indicate that mineralization is structurally controlled, with shear zones, faults, and lithological contacts acting as primary fluid conduits. Geophysical anomalies coincide with hydrothermal alteration zones, felsic intrusions, and pegmatitic bodies, while petrographic evidence confirms deformation-enhanced recrystallization and sulfide mineralization. This integrated study provides a robust exploration model for structurally controlled, basement-hosted mineral systems and defines priority targets for follow-up investigations in southwestern Nigeria and analogous Pan-African terranes.

Keywords: Okemesi, Mineralization, Basement Terrain, Aeromagnetic, Pan-African, Hydrothermal Alteration.

INTRODUCTION

The Okemesi area is located within the southwestern Nigerian Basement Complex, a geologically significant terrain characterized by diverse lithologies, complex structural architecture, and high potential for metallic mineralization [**1**]. The Basement Complex forms part of the Africa-wide orogenic belts and comprises Archean to Early Proterozoic crystalline rocks, including gneisses, schists, quartzites, and granitoids that have been extensively reworked during multiple tectono-metamorphic events [**1,2,3].** The Okemesi district is defined by the Okemesi Fold Belt, a structurally complex province consisting of imbricate thrusts, recumbent folds, and shear zones that enhance permeability and facilitate hydrothermal fluid flow and ore formation [**4, 5].** Gold and base-metal mineralization are widely reported in the deformed basement rocks of southwestern Nigeria [**6, 7**], with auriferous quartz veins in the Okemesi Fold Belt genetically linked to regional deformation

ISSN No. 2454-6194 | DOI: 10.51584/IJRIAS |Volume XI Issue VI June 2026

and shear-related processes [**8, 9**]. Despite this mineral potential, systematic exploration in the area remains limited, and existing geological mapping provides only partial insight into subsurface mineralization controls [**2**]. Geophysical surveys, particularly aeromagnetic methods, are effective in delineating faults, shear zones, and lithological boundaries that control basement-hosted mineralization [**10, 11**], while radiometric data identify potassium (K), thorium (Th), and uranium (U) anomalies commonly associated with hydrothermal alteration [**12].** Geochemical sampling and multi-element analysis, supported by statistical techniques such as factor and cluster analysis, further aid in identifying anomalous zones and pathfinder elements for gold and base metals [**13, 14].** The integration of geophysical and geochemical datasets enhances exploration efficiency by correlating structural features with geochemical enrichments, thereby improving target definition in underexplored basement terrains such as Okemesi [**11].** In the context of increasing global demand for critical metals and Nigeria's drive to diversify its economy through solid mineral development [**9, 15**], a comprehensive evaluation of the Okemesi mineral system is required. While previous studies emphasized the role of Africa-wide deformation and fault systems in controlling mineralization [**1, 13],** geophysical and geochemical datasets have often been treated independently [**16, 17**]. The main objective of this study is therefore to delineate potential mineralized zones in the Okemesi area by integrating geophysical and geochemical data within a mineral systems framework, explicitly targeting the source of metals, ore-forming pathways defined by faults and shear zones, and geological traps such as lithological contacts and alteration zones [**13].** This approach provides a robust basis for assessing basement-hosted metallic mineralization in the Okemesi region.

Location and description of the study area

The study area lies between longitudes 7°45′E and 8°00′E and latitudes 4°52′N and 5°08′N and is characterized by rugged topography with elevations ranging from 350 to 850 m above sea level [**13].** This rugged relief enhances bedrock exposure and reduces regolith cover, improving the reliability of lithological identification and structural measurements during exploration. Prominent features such as Okemesi Peak [**18**] provide extensive fresh outcrops that are critical for detailed lithological mapping and validation of geophysical interpretations. The physiography is structurally controlled, with resistant quartzites and schistose rocks forming ridges and escarpments, while less competent mica schists and weathered horizons occupy valleys, thereby enhancing the surface expression of faults and fractures that act as pathways for mineralization **[1**]. Accessibility is provided by major roads linking Ado-Ekiti, Ijero, and Ilesha, as well as footpaths across valleys and ridges, facilitating efficient geological mapping, ground geophysical surveys, and systematic geochemical sampling [**19]**. The area lies within the Osun River drainage system, where seasonal streams follow structural trends, promoting erosion and exposing basement rocks suitable for stream-sediment and soil sampling [**20**]. The humid tropical climate, with a dry season from November to March and a rainy season from April to October, and annual rainfall of 1200–1600 mm [**21]**, results in intense chemical weathering and the development of ferruginous lateritic profiles that influence geochemical dispersion. However, residual soils and laterites can preserve pathfinder element anomalies, making the terrain favourable for integrated geological, geochemical, and geophysical exploration, with ridge crests optimal for structural mapping and valley floors suitable for regional sampling of base-metal and gold-related anomalies [**22**].

Regional geology

The regional geological architecture of Nigeria **Fig. 1** highlights the spatial distribution of the Precambrian Basement Complex and the surrounding Phanerozoic sedimentary basins [**1, 23]**. The Basement Complex occupies much of western and northern Nigeria and forms part of the Pan-African mobile belt that developed between the West African Craton to the west and the Congo Craton to the southeast [**2, 24]**. This basement is composed of Archean to Early Proterozoic crust that was extensively reworked during the Africa-wide tectonism thermo-tectonic events (~600 Ma), leading to widespread deformation, regional metamorphism, magmatism, and the emplacement of syn- to late-tectonic granitoids [**25, 26**]. Regionally, the Basement Complex is subdivided into the Migmatite-Gneiss Complex, the Schist Belts, and the Africa-wide orogeny Granitoids, reflecting variations in lithology, metamorphic grade, and tectonic evolution [**27, 28].** Within the southwestern part of the Basement Complex lies the Okemesi Fold Belt, which forms part of the Ilesha Schist Belt. This belt is characterized by pronounced structural complexity and significant mineralization potential,

ISSN No. 2454-6194 | DOI: 10.51584/IJRIAS |Volume XI Issue VI June 2026

distinguishing it from adjacent basement domains [**29, 7**]. The lithological assemblage comprises banded and granite gneisses, quartzites, pelitic and psammitic schists, amphibolites, meta-ultramafic rocks, and intrusive granitoids and charnockites [**25, 30**]. Metamorphic conditions range from greenschist to amphibolite facies, with localized granulite facies metamorphism attributed to peak Africa-wide orogeny thermal conditions [**1, 29**]. Structurally, the Ilesha Schist Belt exhibits tight to isoclinal folding, thrusting, and well-developed shear zones with dominant NE–SW trends, reflecting multiple episodes of ductile and brittle deformation [**31, 32].** A key regional structure, the Ifewara–Zungeru Shear Zone, cuts across the Basement Complex and represents a major reactivated Africa-wide tectonism transcurrent fault system. This shear zone plays a critical role in focusing deformation and channeling hydrothermal fluids, thereby enhancing mineralization [**2, 33**]. Geochemical studies indicate enrichment of Au, Pb, Zn, and Cu associated with shear zones, quartz veins, and lithological contacts within the belt [**7, 30**], while airborne geophysical data delineate structurally controlled alteration zones marked by magnetic lows and potassium anomalies [**34**]. Collectively, the regional basement framework underscores the strong tectono-metamorphic control on mineralization in the Okemesi Fold Belt and its significance for structurally hosted metallic mineral exploration within the Nigerian Basement Complex.

Fig. 2 displays a complex basement terrain with lithologies typical of the Southwestern Nigerian Basement Complex [**1, 29, 35**]. Dominant units include migmatite (Mg), banded gneiss (BG), schist (SU), quartzite (Qz), pegmatite (PG), and charnockite (Ch). Migmatites in the northeastern sector (Baba Ori-Oke 8B, Ijero Lepidolite) mark high-grade metamorphic cores, grading westward into schist belts along the principal deformation trend (Ijero–Iloro-Ekiti–Arapate–Odo Owa). Charnockitic intrusions around Ijero and Odo Owa indicate granulite-facies metamorphism post-dating regional deformation, while quartzite ridges (Okemesi, Okela, Ido-Ile) reflect tectonic resistance. Pegmatitic veins intrude schist and charnockite units, and banded gneisses in the northwest (Okemesi, Oke-Ila) represent reworked Archean–Paleoproterozoic basement rocks [**1, 2].** Integration**:** Spatial distribution of lithologies aligns with structural trends, suggesting multiple continental-scale deformation and intrusion events. Schist belts and migmatitic cores correlate with magnetic and radiometric anomalies, while charnockites and pegmatites coincide with lineaments and hydrothermal alteration zones, providing a coherent litho-structural framework for mineralization analysis [**1, 2, 36**]. Implications: The Okemesi–Ijero structural axis, defined by lithological contrasts and deformation patterns, represents the most prospective corridor for hydrothermally controlled mineralization. The association of banded gneisses, pegmatites, and schist with structural lineaments indicates priority zones for targeted exploration, particularly for gold, Sn–Ta, and base-metal mineral systems within the Nigerian Basement Complex [**1, 37]**

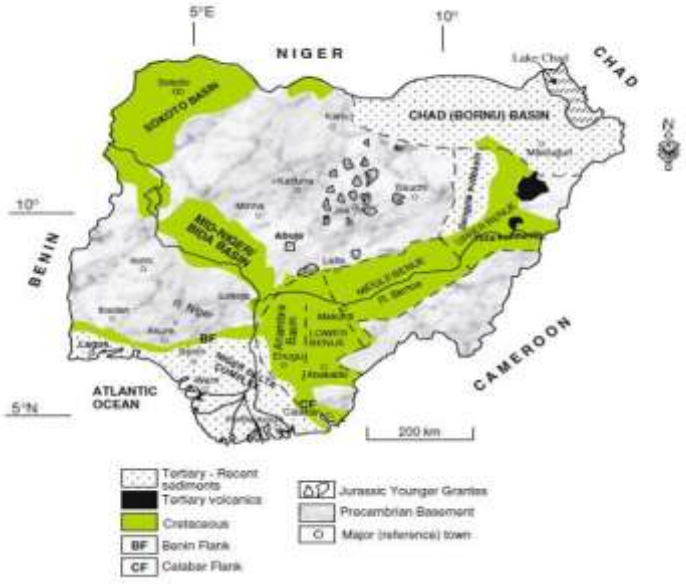

Fig. 1. Geological map of Nigeria showing the major geological Components, Basement, Younger Granites, and Sedimentary Basins **[23].**

ISSN No. 2454-6194 | DOI: 10.51584/IJRIAS |Volume XI Issue VI June 2026

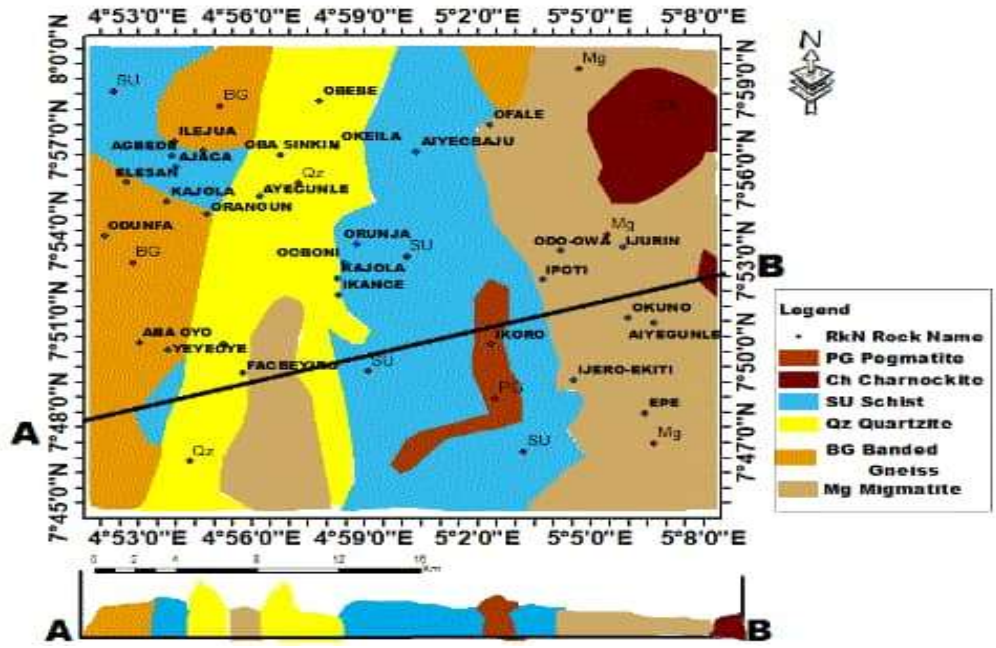

Fig. 2. Geological and cross-sectional map of the study area showing the distribution of rock units and their structural relationships. The map illustrates surface lithological variations, while the cross-section depicts subsurface geometry and structural features such as faults and contacts.

Aeromagnetic dataset materials and methods

The primary dataset used in this study comprises high-resolution aeromagnetic data acquired by the Nigerian Geological Survey Agency **[25]**, as part of the 2006–2007 national airborne geophysical survey conducted by Fugro Airborne Surveys. The data correspond to the Ado-Ekiti Sheet 244 and are provided in gridded Total Magnetic Intensity (TMI) format at a scale of 1:100,000, suitable for regional geological interpretation and basement structural mapping. The survey employed NE–SW and –oriented flight lines spaced at 150 m, with control tie lines at wider spacing for leveling and correction. Data acquisition was performed at a nominal flight altitude of 50 m, providing high-resolution magnetic sampling across the crystalline basement terrain **[1].** The final grid was generated with a cell size of 250 m to emphasize regional magnetic signatures. All data processing, filtering, and enhancements were performed using Geosoft Oasis Montaj™ version 8.4**,** and map production, transformation algorithms, and structural interpretation were executed using the software's geophysical processing modules **[33].**

IGRF Correction

To isolate local magnetic anomalies caused by subsurface sources, the International Geomagnetic Reference Field **[26]** was used to remove the regional geomagnetic field contribution. The corrected TMI is expressed as:

$$\Delta B(X, Y) = \text{TMI measured } (X, Y) - \text{IGRF } (X, Y) \ldots\ldots\ldots\ldots\ldots\ldots (1)$$

where:

$TMI_{measured}(x,y)$ = recorded magnetic field

IGRF(x,y)= main geomagnetic field at location (x, y)

Total Magnetic Intensity (TMI) Map

The Total Magnetic Intensity (TMI) map represents the combined magnetic response of all subsurface sources [**8**]. Following IGRF correction, the TMI field reflects residual magnetic anomalies attributable to variations in lithology and structural features within the study area and is defined as:

ISSN No. 2454-6194 | DOI: 10.51584/IJRIAS |Volume XI Issue VI June 2026

$$TMI\,(X,Y) = \sqrt{X}(x,y)2 + Y\,(x,y)2 + Z\,(x,y)2 \ldots\ldots\ldots\ldots\ldots\ldots\ldots (2)$$

Where X, Y, Z are the north, east, and vertical components of the measured magnetic field, respectively [**8].**

The TMI map serves as the baseline for all subsequent enhancement procedures.

Filtering Methods

To enhance geological features, the TMI data were subjected to spectral filtering to separate regional and residual magnetic anomalies. A Butterworth filter was applied in the frequency domain to suppress long-wavelength regional signals and enhance short-wavelength anomalies related to shallow structures. The high-pass component emphasized near-surface magnetic sources such as faults and fractures, while the low-pass component highlighted deep-seated regional trends [**18]**. The resulting residual magnetic map clearly delineated structural features used for subsequent lineament analysis. It is expressed as:

$$M\,residual\,(kx,ky) = M(kx,ky) * 1 / (1 + (kc / k)\text{^}n) \ldots\ldots\ldots\ldots (3)$$

where:

M (kx, ky) = Fourier transform of TMI

k = wave number

kc = cutoff wave number separating regional and residual components

n =3, the filter order used to obtain the residual map in this study

High-pass filtering highlights shallow, short-wavelength anomalies, while low-pass filtering emphasizes broader regional trends.

Reduction to the Equator (RTE)

At Nigeria's low magnetic latitude (~5–10°N), magnetic anomalies are laterally displaced [**38]**. Reduction to the Equator (RTE) corrects this shift, repositioning anomalies directly above their causative sources. This process improves the interpretability of both shallow and deep magnetic features, allowing more accurate delineation of structural trends in the study area. This is expressed as:

$$RTE\,(k) = F * TMI\,(k) * (i * kx + d * ky) / |k| \ldots\ldots\ldots\ldots\ldots\ldots\ldots (4)$$

where:

kx, ky = wave numbers in x and y directions

i = inclination of the geomagnetic field

d = declination of the geomagnetic field

F = total geomagnetic field intensity

Residual magnetic anomaly

Filtering was applied to the magnetic dataset to isolate localized anomalies and remove regional trends, generating the residual magnetic anomaly map. A high-pass filter was used to emphasize short-wavelength variations associated with near-surface lithological contacts, shear zones, and mineralized bodies, while suppressing broad regional signals. This approach ensures that subtle magnetic anomalies are accurately highlighted for structural and exploration interpretation. A grid cell size of 50 × 50 m and a filter cutoff

ISSN No. 2454-6194 | DOI: 10.51584/IJRIAS |Volume XI Issue VI June 2026

wavelength of 2 km were adopted, following standard procedures for basement terrains [**16, 39, 48**]. The filtered residual map provides enhanced visualization of structurally controlled magnetic variations, improving target prioritization in the study area.

$\Delta T\_\{residual\}(x,y) = \Delta T\_\{observed\}(x,y) - \Delta T\_\{regional\}(x,y)$……..... (5)

ΔT_residual (x, y) = residual magnetic anomaly at location (x, y)

ΔT_observed (x, y) = measured total magnetic intensity at location (x, y)

ΔT_regional (x, y) = regional or long-wavelength magnetic field at location (x, y)

Analytical Signal

The Analytical Signal (AS) resolves directional ambiguity and enhances the edges of magnetic anomalies independently of magnetization direction. Maxima in AS amplitude clearly delineate the boundaries of magnetic bodies, improving the definition of shallow and deep structures in equatorial terrains. This facilitates accurate mapping of lineaments and structural trends [**50**]. It is expressed as:

$$AS = \sqrt{[(\partial M/\partial x)^2 + (\partial M/\partial y)^2 + (\partial M/\partial z)^2]} \quad \text{……. (6)}$$

Analytical signal amplitude maxima directly outline the edges of magnetic bodies, improving boundary definition in equatorial terrains

Euler Deconvolution

Euler Deconvolution was applied to quantitatively estimate the locations and depths of magnetic sources. Structural indices (SI) of 0.5, 1, and 0.5–1 were used to delineate geological contacts, faults, and intrusive bodies, respectively [**40],** ensuring realistic depth solutions for shallow sources consistent with field observations and structural trends. A window size of 3 × 3 cells**,** depth tolerance of 10%**,** and maximum acceptable horizontal clustering distance of 500 m were adopted for the analysis, following standard procedures for basement terrains [**40**]. The method provides depth solutions and source positions, enabling precise mapping of lineaments and structural controls in the study area.

$(x - xo)(\partial M/\partial x) + (y - yo)(\partial M/\partial y) + (z - zo)(\partial M/\partial z) = N(B - M)$…….... (7)

where:

(x0, y0, z0) = source location

N = structural index (S

B = regional/background field

M = measured magnetic anomaly

Materials and methods for the radiometric dataset

The radiometric survey for the Okemesi area, Ekiti State, was conducted using high-resolution airborne gamma-ray spectrometry at a scale of 1:100,000. The dataset comprises Potassium (K%), Thorium (Th ppm), and Uranium (U ppm) grids, which were processed to evaluate alteration signatures and assess potential associations with felsic intrusive bodies. The primary objective was to identify geochemical indicators of hydrothermal activity, particularly potassic alteration, which is commonly associated with Au–Cu mineralization systems [**12].**

ISSN No. 2454-6194 | DOI: 10.51584/IJRIAS |Volume XI Issue VI June 2026

Potassium Deviation Analysis

Potassium anomaly intensities were quantified using the Potassium Deviation Index (KD) following the equation:

$$KD = (K - Kmean) / Ksd \quad \ldots\ldots (8)$$

where K represents the value of each grid cell, Kmean is the mean of the dataset, and Ksd is the standard deviation. Zones with KD > +1 were interpreted as significant potassic alteration halos of exploration relevance. Spatial analysis of the KD map highlighted high-intensity potassium zones coinciding with felsic intrusions, indicating potential loci for hydrothermal Au–Cu mineralization. Integration with Th and U grids allowed further discrimination of magmatic versus hydrothermal signatures, as Th enrichment typically reflects felsic magmatic contributions, while elevated U indicates hydrothermal mobilization [**36].**

The radiometric grids were processed and analyzed using standard GIS techniques to produce anomaly maps, which were subsequently interpreted in the context of lithology, structural trends, and known mineral occurrences in the Okemesi area.

Integrated Interpretation

All data processing, filtering, and modeling were carried out in Geosoft Oasis Montaj 8.4**.** The integration of aeromagnetic and radiometric datasets enabled:

- Structural framework reconstruction
- Lithological boundary mapping
- Identification of potassic and radiogenic alteration halos
- Recognition of fluid pathways and mineralization targets

This combined approach provides a robust basis for defining priority zones for follow-up geological mapping, sampling, and drilling.

Field and laboratory materials and methods

For geological mapping in Okemesi and its environs, the materials used included a compass, clinometer, field notebook, topographic/base map, ruler, protractor, pencils (colored and regular), hand lens, digital camera, geological hammer, chisel, sample bags, measuring tape, and safety clothing (solid shoes, gloves, hat, sunglasses, and backpack). These facilitated accurate observation, documentation, and sample collection.

The study began with a reconnaissance survey using a 1:25,000 scale map, followed by systematic geological mapping. Outcrops were located, and GPS coordinates were recorded using a Garmin GPSMAP 64s handheld GPS device, ensuring accurate spatial positioning of sampling points **[14].** Observations included megascopic mineral identification, texture, color, weathering, strike, and dip measurements, and sketching in the field notebook. Representative samples were collected from the major rock units identified during field mapping, including migmatite (Mg), banded gneiss (BG), schist (SU), quartzite (Qz), pegmatite (PG), and charnockite (Ch). A total of 36 rock samples were collected at approximately 500 m intervals at an average density of one sample per 4 km², with 18 fresh samples selected for subsequent petrographic analysis based on the following criteria**:**

1. Lithological representativeness across all major rock units
2. Presence of alteration/mineralization features indicative of hydrothermal processes
3. Spatial distribution to cover both structurally controlled and potentially mineralized zones

ISSN No. 2454-6194 | DOI: 10.51584/IJRIAS |Volume XI Issue VI June 2026

This approach ensured that the selected samples adequately captured the lithological and alteration variability while targeting areas with potential mineralization.

Petrographic analysis was conducted at the Petrology Laboratory of Ajayi Crowther University, Oyo. Rock samples were transported to the laboratory and prepared for analysis using a diamond saw, lapping machine, and hydraulic rock splitter, with size reduction achieved using Swing-Jaw, Boyd, and Vibratory Ring Mills. Samples (~2 × 1 × 0.5 cm) were ground with silicon carbide, baked at 120 °C on an electric thermal plate, and mounted on glass slides using Araldite epoxy. Specimens were then thinned to 0.5 mm, cleaned, dried, and covered with glass slips using Canada balsam. Thin sections of migmatite (Mg), banded gneiss (BG), schist (SU), quartzite (Qz), pegmatite (PG), and charnockite (Ch) were examined under a research petrographic microscope and an ore microscope for polished sections to determine mineral composition, texture, grain size, and microstructures. Observations facilitated systematic mineral classification, confirmation of rock types, and assessment of metamorphic grade. Expendables used included mounting epoxy, flat glass, petrographic slides, and grinding oil.

For geochemical analysis, approximately 0.25 g of each pulverized sample underwent partial multi-acid digestion (4A-MS) at ACME Analytical Laboratories Ltd., Vancouver, Canada. Trace elements were measured using ICP-MS (detection limits 0.01–1 ppm), and gold concentrations were determined using fire assay with atomic absorption spectrometry (1E-LR, detection limit 0.01 ppm) [**43**]. All sample masses are now consistently reported in grams, and the procedures ensure reliable, reproducible, and representative geochemical data.

The geochemical dataset was statistically processed to identify element associations, anomalous zones, and lithological controls relevant for hydrothermal and intrusion-related mineralization [**31]**. Data analysis was performed using ROCKWORKS and SPSS version 18. Initially, descriptive statistics—including mean, standard deviation, and coefficient of variation—were computed to evaluate the distribution, variability, and potential outliers of trace elements across the study area. Subsequently, multivariate techniques, including correlation analysis and factor analysis, were applied to reveal geochemical patterns, group samples with similar characteristics, and explore associations between elements and lithological units [**23]**. Given the relatively small sample size, multivariate results are interpreted qualitatively, with high correlation coefficients considered indicative trends rather than definitive geochemical linkages [**29].** This approach ensures that the statistical methods are directly tied to the study objectives, providing a robust framework for interpreting the relationships between geochemistry, lithology, and mineralization potential in the Okemesi basement terrain [**30].**

RESULTS AND DISCUSSION

Aeromagnetic maps

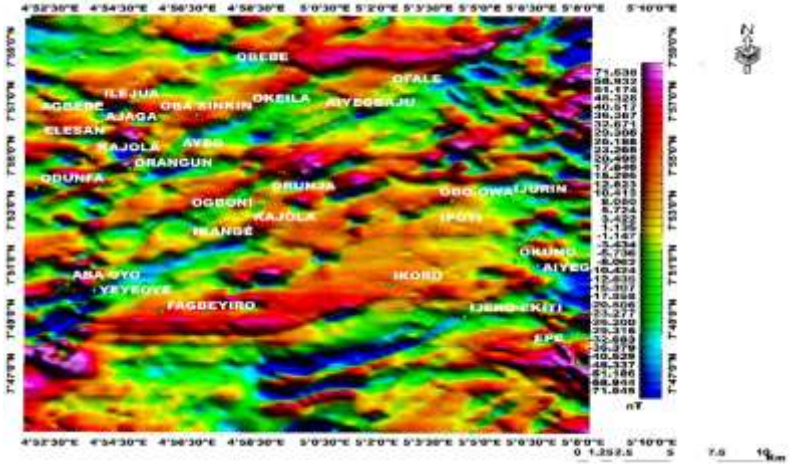

Fig. 3. Total Magnetic Intensity (TMI) map of the study area showing spatial variations in magnetic responses, highlighting major lithological units, structural trends, and potential zones of mineralization.

ISSN No. 2454-6194 | DOI: 10.51584/IJRIAS |Volume XI Issue VI June 2026

Spatial variations in magnetic signatures reflect contrasts in basement lithology, structures, and mineralization potential. High magnetic intensity zones (red–pink to purple) around Ile-Iju, Oba-Sinkin, Oke-Ila, Obebe, Fagbejiro, Aba Oyo, and Ikoro are interpreted as magnetite-rich rocks, including mafic intrusives, amphibolites, and iron-rich gneisses, commonly associated with hydrothermal systems and structurally controlled orogenic gold [**42, 43].** Low magnetic zones (green–blue) around Ipoti, Odo-Owa, Okuno, Aiyegunle, and Ijero-Ekiti correspond to felsic granites and migmatitic gneisses, typically poor in ferromagnetic minerals [**41**, **44**]. Integration of TMI patterns with linear trends and sharp gradients highlights structurally controlled mineralization. Linear anomalies around Kajola, Ikange, Ogbomi, Orunja, and Aye-Gbaju delineate shear zones, faults, and lithological contacts. These features complement geological and geochemical evidence, High-intensity and structurally complex zones, especially the Ile-Iju–Oke-Ila–Fagbejiro and Kajola–Ikange corridors, are priority targets for exploration. These areas warrant detailed ground-based geophysical surveys and focused geochemical studies to delineate structurally controlled, economically viable mineralization (**Fig. 3**).

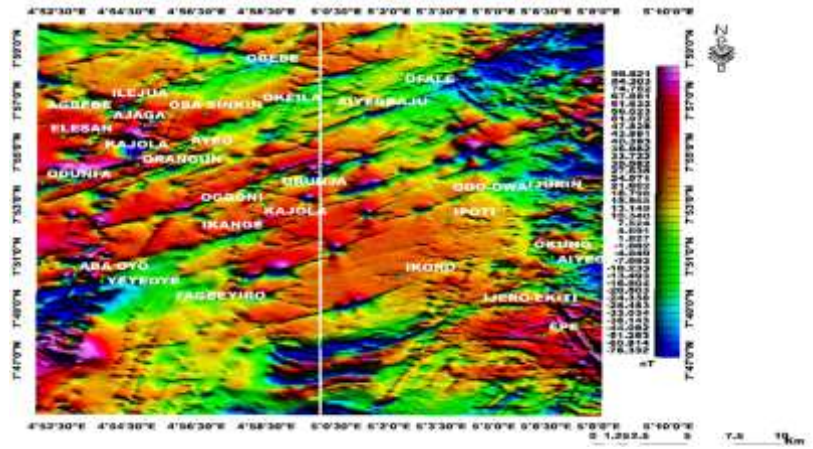

Fig. 4. Reduced-to-equator (RTE) magnetic map of the study area illustrating spatial variations in magnetic intensity, delineation of lithological boundaries, and prominent structural trends such as faults and shear zones. The map highlights linear and curvilinear anomalies that reflect subsurface geological structures and deformation patterns. These magnetic signatures indicate areas of structural complexity and potential pathways for hydrothermal fluid flow, suggesting zones favourable for metallic mineralization.

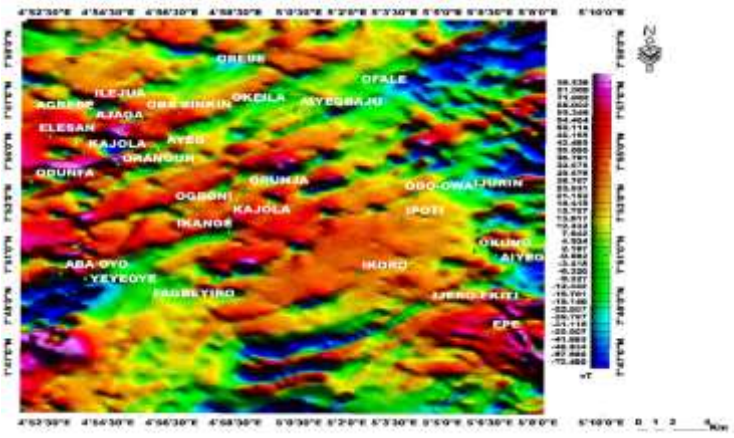

Fig.5. Residual magnetic anomaly map of the study area highlighting localized variations in magnetic intensity after removal of the regional field. The map delineates subtle and short-wavelength anomalies associated with near-surface geological features, including faults, fractures, and lithological contacts. These anomalies emphasize zones of structural complexity and potential hydrothermal alteration, thereby indicating prospective areas for metallic mineralization within the study area.

Variations in basement lithology, structural fabric, and deformation are expressed by alternating high- and low-intensity magnetic zones [**1, 3**]. Positive anomalies (pink–red) around Kajola, Ogbon, Ayegunle, Ikoro, and

ISSN No. 2454-6194 | DOI: 10.51584/IJRIAS |Volume XI Issue VI June 2026

Ijero-Ekiti correspond to magnetite-rich amphibolites, banded gneisses, and basement intrusives associated with Africa-wide tectono-magmatic activity**.** These highs are linked to deep-seated structures that likely channel mineralizing fluids. Low anomalies (blue–green) across Igbajo, Aba Oyo, Ayegbaju, Igbara-Odo, and Odo-Owa indicate fractured and altered zones, representing shear zones, faults, and fold hinges favorable for hydrothermal gold and sulphide mineralization [**46, 47, 48**]. Linear magnetic trends align with regional deformation controlled by the Ifewara–Zungeru Shear Zone [**45**, **49**]. Magnetic breaks around Ayetoro, Ogbese, Ikogosi, and Araromi mark fault segments and structural intersections. . Areas where magnetic highs intersect structural discontinuities represent priority targets for ground-based geophysical and geochemical surveys to delineate economically viable orogenic gold mineralization (**Fig. 4**).

Shallow magnetic features are emphasized by suppressing regional magnetic effects, thereby isolating signatures related to magnetite- and pyrrhotite-bearing mineralization [**50, 51**]. Residual amplitudes range from −48.60 nT to +41.50 nT, with strong positive anomalies (red–magenta) around Kajola, Ikange, Ikorod, Ijero-Ekiti, Epe, Elesan, and Aba Oyo. These anomalies indicate iron-rich lithologies such as banded iron formations or mafic–ultramafic intrusions, which are favorable for Fe, Cu, Ni, and structurally controlled Au mineralization [52, 6, 53]. Elongated anomalies trending along major fractures are interpreted as magnetic dykes or veins, serving as pathways for mineralizing fluids [2, 50]. Negative anomalies (blue) adjacent to magnetic highs, particularly south of Aba Oyo and Elesan, reflect dipping bodies and structural disruption [**54**]. Sharp contrasts delineate shear zones and lithological contacts are known to localize mineralization [**55**]. Residual highs correlate with previously mapped high-signal zones, confirming shallow, laterally continuous, and structurally controlled magnetic sources. Positive residual anomalies along principal deformation trends, especially around Kajola, Ikange, Ikorod, and Ijero-Ekiti, represent priority targets. These zones are recommended for detailed ground geophysical surveys and exploration drilling to delineate shallow, structurally controlled metallic and/or orogenic gold mineralization (**Fig. 5**).

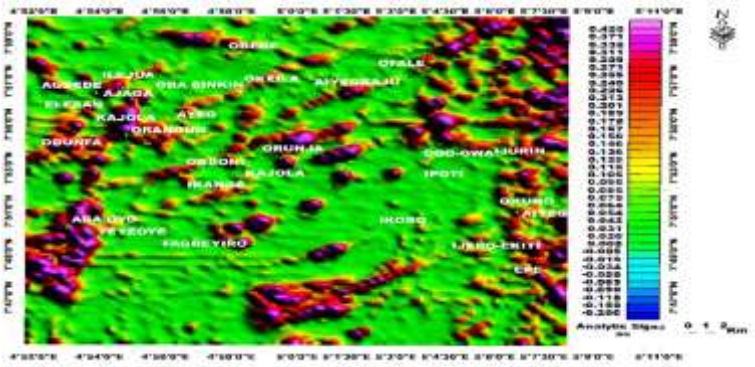

Fig. 6. Analytical signal map of the study area highlighting the edges of magnetic source bodies and lithological boundaries. The map enhances the delineation of faults, contacts, and structural discontinuities irrespective of magnetization direction. These features indicate zones of structural control and potential mineralization within the study area.

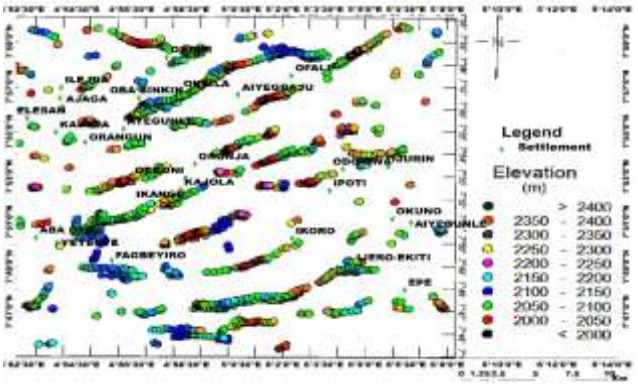

ISSN No. 2454-6194 | DOI: 10.51584/IJRIAS |Volume XI Issue VI June 2026

Fig. 7. Euler deconvolution map of the study area showing the spatial distribution and estimated depths of magnetic source bodies. The solutions delineate subsurface structural features such as faults, contacts, and intrusive bodies. These depth-constrained anomalies provide valuable insight into structural controls and potential zones of mineralization.

Fig. 6 highlights magnetic contrasts reflecting lithological variations and structural complexity. High AS amplitudes around Aba Oyo, Yeyeoye, and parts of Ayegunle indicate shallow, strongly magnetic sources such as magnetite-bearing mafic intrusives, iron formations, or magnetic sulphide-rich lithologies [**1, 46, 3**]. These elevated magnetic gradients suggest favourable settings for iron oxide, base-metal sulphide, and structurally controlled orogenic gold mineralization linked to continental-scale deformation, magmatic and tectonic events. High AS anomalies align with principal deformation trends consistent with the Ifewara–Zungeru Shear [**50, 47].** The spatial coincidence of high AS amplitudes with fracture networks and anomaly intersections reinforces a structurally focused metallogenic model **[49].** Low to moderate AS areas, including Ipoti and Ikoro, correspond to weakly magnetic granitic or gneissic units, less favourable for magnetite-rich mineralization but requiring geochemical verification [**27].** Zones of high AS amplitudes and structural intersections, particularly around Aba Oyo, Yeyeoye, and Ayegunle, represent priority exploration targets. These areas warrant detailed ground geophysics and geochemical surveys to delineate economically viable, structurally controlled mineralization, including orogenic gold.

Fig. 7 constrains the depth and geometry of magnetized sources in the Okemesi Fold Belt [**56].** Shallow red solutions, concentrated around Oba Sinkin, Orunja, and Odo-Owa–Iurin along belt-parallel structures, indicate iron-rich formations, mafic intrusions, or sulphide-bearing units with high magnetic susceptibility **[1**]. These shallow sources represent high-priority targets for structurally hosted iron, gold, and base-metal (Zn, Cu) sulphide mineralization [**46, 3**]. ED solutions correlate closely with mapped lineaments, highlighting the control of the regional structural framework on mineralized bodies. Major shear zones, including the Ifewara–Zungeru system, likely acted as fluid pathways hosting gold-bearing quartz veins [**50, 47**]. Shallow, structurally aligned ED sources around Oba Sinkin, Orunja, and Odo-Owa–Iurin indicate high potential for metallic mineralization. These zones are recommended for detailed ground geophysics and exploration drilling to delineate economically viable, structurally controlled deposits, particularly orogenic gold [**38, 40, 57].**

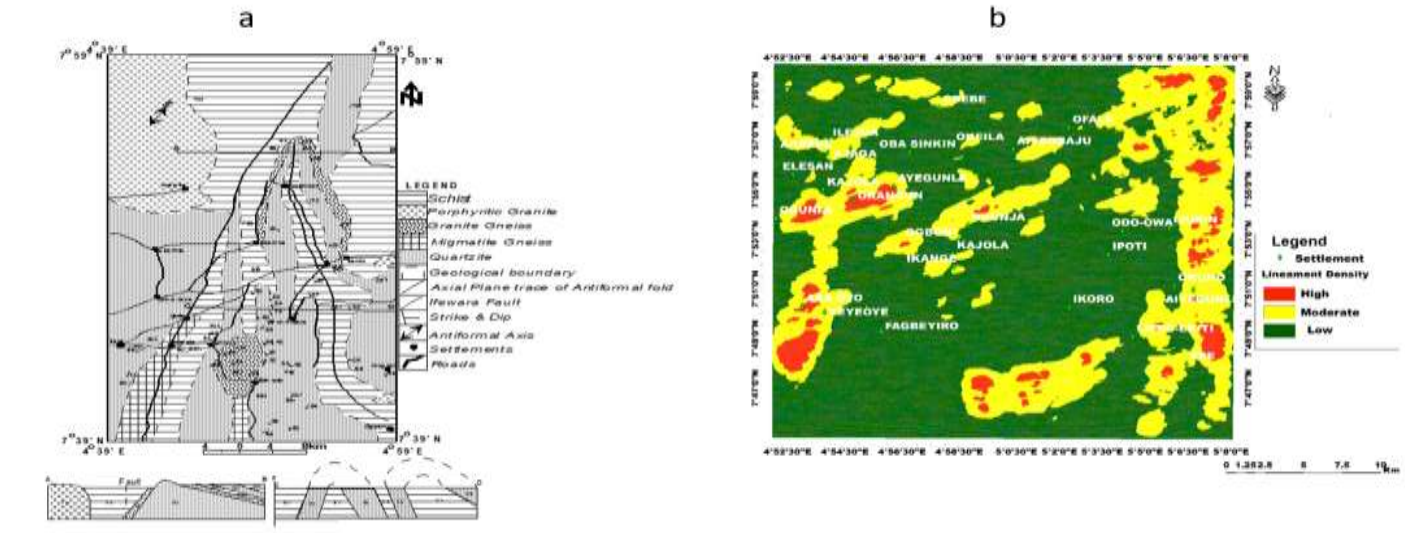

Fig. 8. (**a**)Structural map of the Okemesi area depicting major lineaments, fault orientations, and fold patterns within the basement terrain **[24]. (b)** Lineament density map of the study area illustrating the concentration and spatial distribution of structural features.

Fig. 8a is dominated by principal deformation trending Africa-wide orogeny structures, with subordinate structural orientations. These lineaments represent major faults, folds, and fracture zones previously mapped by [**56**, **24, 58].** The NE–SW structures reflect the primary tectonic stress regime associated with the Africa-

ISSN No. 2454-6194 | DOI: 10.51584/IJRIAS |Volume XI Issue VI June 2026

wide orogeny, while the principal deformation trends indicate secondary reactivation events or cross-cutting fractures. High-density zones on the aeromagnetic map. **Fig. 8b** coincide with the dominant structures in the northern and central parts of the study area, whereas moderate-density zones (yellow) align with principal deformation trends [**59, 60, 61**]. Low-density regions (green) correspond to relatively undeformed areas or zones with subdued structural expression. Comparison of the aeromagnetic lineament density map with previously mapped structural data demonstrates a strong correlation between high lineament density zones and major dominant structural orientation faults and folds **[2, 6].** This integration confirms the continental-scale deformation origin of these structures and reveals previously underrepresented secondary fault and fracture networks [**1, 2**]. Moreover, the aeromagnetic data help identify previously undetected lineaments, highlighting the value of combining geophysical and geological datasets to enhance structural mapping accuracy. The integrated structural framework indicates that the Okemesi area is a structurally complex terrain with interacting fault, fold, and fracture systems **[24].** These findings provide a detailed characterization of structural trends and density variations, which can serve as a foundation for further geoscientific investigations in the region [**24, 25].**

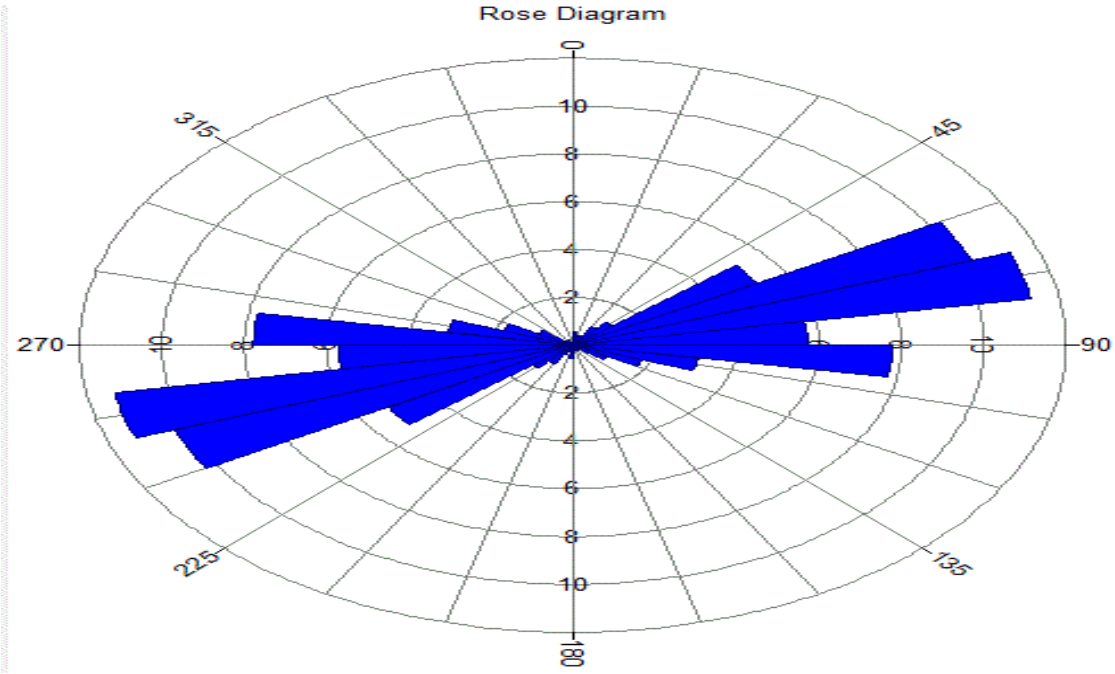

Fig. 9 Rose Diagram showing the frequency distribution of structural orientations measured in the study area. The diagram illustrates the dominant strike directions of geological features such as joints, fractures, and foliations.

Fig. 9 illustrates the dominant structural orientations of mapped lineaments in the study area, providing insight into the tectonic regime. The longest petals indicate a strong Northeast–Southwest (NE–SW) structural trend (approximately 45°–75° and 225°–255°), representing the most frequent and persistent lineaments. A secondary but significant Northwest–Southeast (NW–SE) trend (approximately 300°–330° and 120°–150°) is also observed. These two orthogonal sets suggest that deformation within the area was largely influenced by Pan-African tectonism, which imposed major shear zones and conjugate fracture systems across the Nigerian Basement Complex [**1, 33].**

Structurally, these lineaments represent deep-seated fault and fracture zones, indicating potential pathways for magmatic and hydrothermal fluids. Minor N–S and E–W trends may reflect later brittle reactivation or secondary fracturing due to ongoing intraplate stresses [**55].** The Rose Diagram confirms that the geological structures in the study area are dominantly aligned NE–SW, with subsidiary NW–SE trends. These structural orientations provide a robust framework for understanding deformation patterns, and intersections of major lineaments could be considered for further investigation where geochemical or geophysical anomalies are present [**6, 53, 56**].

ISSN No. 2454-6194 | DOI: 10.51584/IJRIAS |Volume XI Issue VI June 2026

Radiometric data

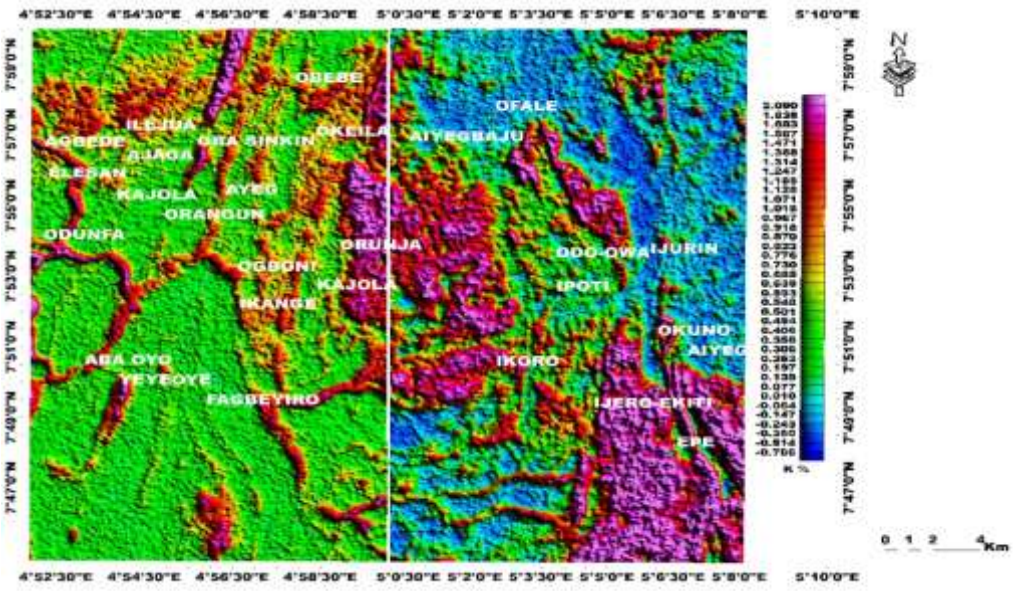

Fig. 10. Potassium (K) anomaly map of the study area showing geochemical variations and zones of elevated K concentration. High K values highlight felsic intrusions and potassic alteration associated with hydrothermal processes. These anomalies help identify potential structurally controlled mineralization zones within the basement complex.

As shown in **Fig. 10,** the distribution of Potassium (K) anomalies highlights shallow lithological variations that are useful for understanding rock types and structural control [**62, 63**]. High K values (1.49–4.66) occur in the northwestern sector (Obebe, Ile-Iju, Oba Sinkin), central-eastern areas (Orunja, Ipoti, Ikorod), and southeastern parts near Epe, corresponding to K-rich felsic lithologies, including granites and granitic gneisses enriched in K-feldspar and biotite [**54, 1**]. Petrographic observations of thin sections from these areas reveal sericitization, K-feldspar alteration, and mica enrichment, indicating that some high-K zones may reflect hydrothermal modification in addition to primary lithology. Low K anomalies (−0.576 to 0.533) around Aba Oyo and Yeyeoye correspond to K-poor mafic–ultramafic lithologies [**6, 55**], while moderate K zones likely reflect mixed or transitional lithologies along structural corridors. Integration of K anomalies with magnetic, structural, and petrographic data improves lithological discrimination and identifies K-bearing zones. Observed intersections of high-K zones with structurally complex areas can guide further field mapping, geochemical sampling, and alteration studies, while recognizing that K enrichment may result from both primary lithology and hydrothermal processes [**52, 69].**

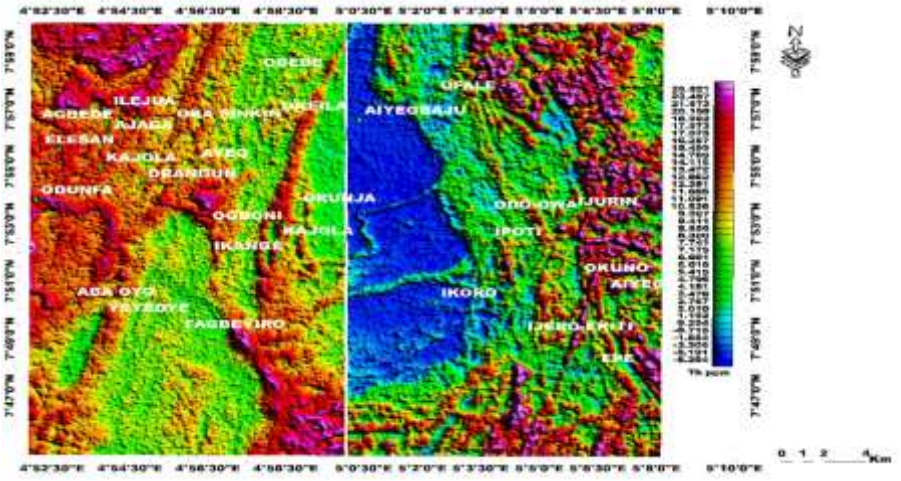

Fig. 11. Thorium (Th) anomaly map of the study area showing geochemical variations and zones of high Th

ISSN No. 2454-6194 | DOI: 10.51584/IJRIAS |Volume XI Issue VI June 2026

concentration. Elevated Th values highlight areas influenced by felsic intrusions and radioactive mineralization. These anomalies help identify potential targets for exploration within the basement complex.

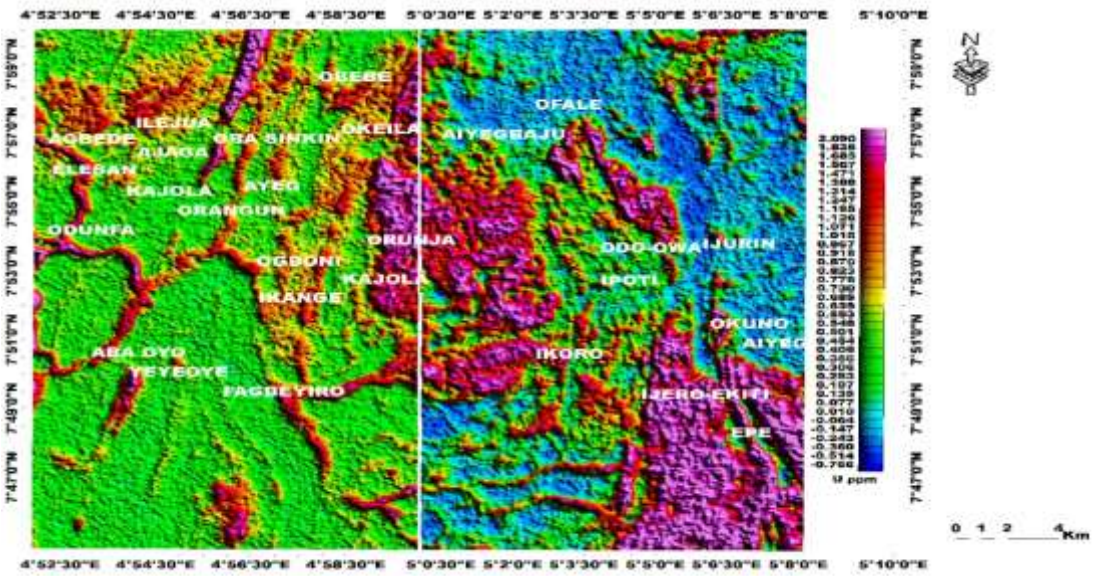

Fig. 12. Uranium (U) anomaly map of the study area showing geochemical variations and zones of elevated U concentration. High U values indicate areas influenced by felsic intrusions and potential radioactive mineralization. These anomalies are useful for identifying prospective zones within the basement complex.

Fig. 11 highlights near-surface lithological variations and Th distribution patterns [**63, 65**]. High Th anomalies in the western sector around Elesan, Odunfa, and Aba Oyo correspond to Th-enriched felsic rocks, such as granites and pegmatites, which contain accessory minerals like monazite, relevant for rare-earth element studies [**1, 6, 66**]. Petrographic analysis of samples from these areas confirms the presence of Th-bearing accessory minerals, including monazite and zircon, indicating that Th anomalies are associated with specific lithologies rather than exclusively reflecting hydrothermal processes.

Low-Th zones in the central-eastern area (Offale–Orunja–Ikorod) correspond to Th-poor mafic or metasedimentary lithologies. Localized Th enrichment along structural zones may reflect lithological contacts or fluid pathways, but the contribution of hydrothermal modification is interpreted cautiously [**65**]. Overlap of low-Th zones with elevated K values and magnetic features may suggest minor hydrothermal influence, while transitional Th zones reflect mixed lithologies or lithological boundaries. Integration of Th anomalies with K, magnetic, and petrographic data improves lithological discrimination and provides a framework for prioritizing further field mapping, geochemical sampling, and detailed petrographic studies [**52, 69**].

Fig. 12 illustrates shallow lithological variations and possible hydrothermal influence [**63, 64, 66**]. High U anomalies around Obebe, Ile-Iju, Elesan, and scattered zones toward Odo-Owa–Ijurin, Ijero-Ekiti, and Epe correspond to U-bearing granitic intrusions and pegmatites, which may host accessory phases such as uraninite and other REE-bearing minerals [**1, 6].** Petrographic analysis confirms alteration features, including minor sericitization and uraninite-bearing accessory phases, suggesting that U anomalies reflect both primary lithology and localized hydrothermal modification. Low-U zones in the central-eastern area (Ayegunle–Orunja–Ikorod) correspond to mafic/ultramafic lithologies.

Transitional U zones along structural corridors likely indicate mixed lithologies or lithological contacts rather than definitive mineralization [**67, 68].** Integration of U, K, Th, and magnetic data, supported by petrographic observations, improves the understanding of lithological variation, alteration patterns, and structural fluid pathways, providing a framework for guiding further detailed field mapping and geochemical sampling [**65, 66, 69].**

ISSN No. 2454-6194 | DOI: 10.51584/IJRIAS |Volume XI Issue VI June 2026

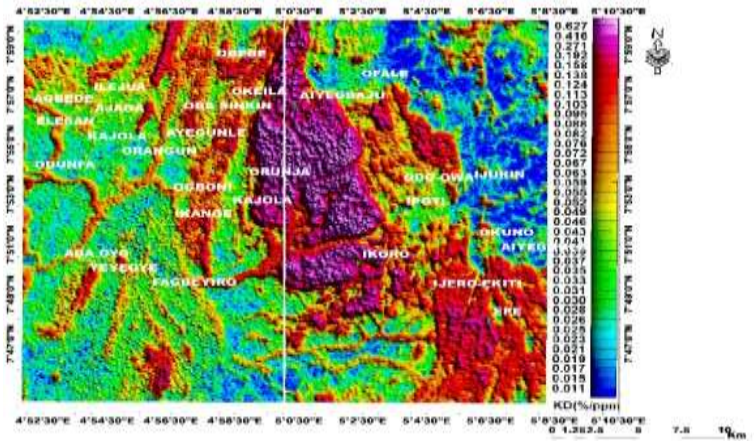

Fig. 13. Potassium (K) deviation map of the study area showing areas with significant variations from background K levels. Elevated deviations highlight geochemical anomalies associated with felsic intrusions and hydrothermal alteration. These zones help identify potential targets for mineral exploration within the basement complex.

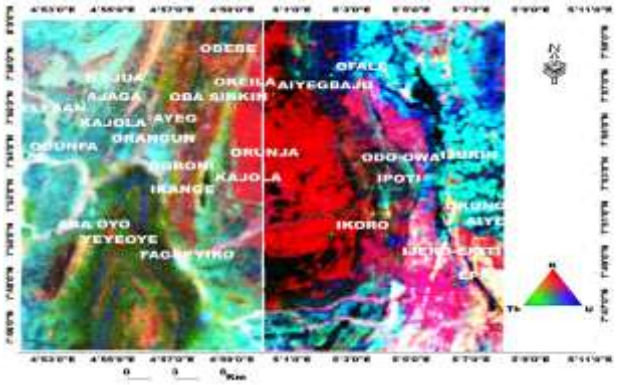

Fig. 14. Ternary map of the study area illustrating the relative distribution of potassium (K), thorium (Th), and uranium (U). The map highlights geochemical associations and contrasting elemental enrichments. These patterns help identify zones of potential mineralization within the basement complex.

Fig. 13 shows the spatial distribution of radiometric anomalies in relation to structural lineaments and magnetic features, highlighting potential fluid pathways and lithological variations [**66, 63].** Low-K areas within mafic intrusions coinciding with magnetic highs correspond to K-poor lithologies rather than definitive Ni–Cu sulfide mineralization [**70]**. Central high-K zones with surrounding moderate-K halos likely reflect variations in granitic intrusions or zones affected by potassic alteration, consistent with hydrothermal modification [**71].** Peripheral moderate-K zones and structural corridors indicate transitional lithologies or zones of mixed radioelement enrichment. The combined K, Th, and U patterns, along with structural alignment, provide a framework for understanding lithological zoning and alteration trends, which may guide detailed geophysical, geochemical, and petrographic follow-up studies in the Okemesi Fold Belt [**66, 75].**

Fig. 14 integrates K, Th, and U anomaly maps with magnetic and structural datasets, highlighting lithological variations and structural trends **[72, 1, 73**]. Spatial coincidence of K- and U-enriched zones with major lineaments likely reflects structurally controlled fluid migration, supported by thin-section observations showing sericitization, K-feldspar alteration, and accessory mineral enrichment. Th-rich zones correspond to felsic lithologies, such as granitic intrusions, rather than directly indicating mineralization [**72]**. Clusters of Euler Deconvolution solutions align with lithological boundaries, especially Schist–Gneiss contacts, indicating faults and shear zones that may serve as potential fluid pathways. N–S elongated units reflect regional deformation, while granite and charnockite intrusions mark late-stage emplacement, providing a framework for understanding structural and lithological controls without overinterpreting mineralization [**69, 75].**

ISSN No. 2454-6194 | DOI: 10.51584/IJRIAS |Volume XI Issue VI June 2026

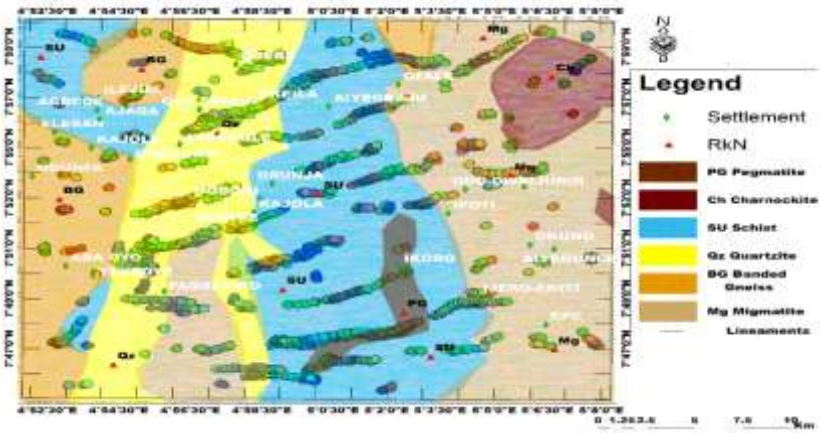

Fig. 15. Euler deconvolution results superimposed on the geologic map of the study area, showing estimated depths and locations of magnetic sources. The results reveal correlations between magnetic anomalies, lithologies, and structural features. These insights help identify potential subsurface mineralization zones within the basement complex.

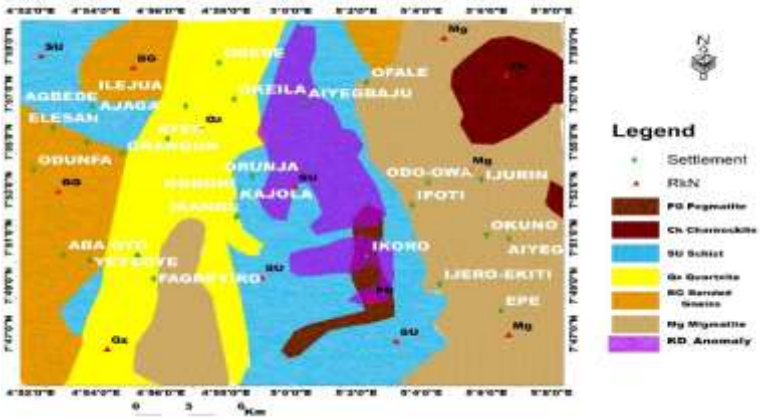

Fig. 16. Potassium (K) deviation map superimposed on the geological map of the study area, highlighting areas of significant K enrichment. Elevated K zones correspond to specific lithologies and potential hydrothermal alteration. These patterns help identify prospective targets for mineral exploration within the basement complex.

Fig. 15 shows the distribution of lithological contacts and pegmatite intrusions, emphasizing structural and lithological controls [**74, 75].** Clusters around Ijero, Oke-Ila, and Odo-Owa coincide with late-stage pegmatite dykes, highlighting potential corridors for rare-metal enrichment (Ta–Nb–Sn–Li) along shear zones and contacts, without asserting confirmed mineralization. Integration of structural, lithological, and geophysical datasets supports interpretation of subsurface patterns and hydrothermal influence [**76, 77**]. Potassium Deviation (KD) anomalies indicate areas of potassic metasomatism, marked by K-feldspar, biotite, and sericite alteration, whereas negative KD values reflect K-depletion or albitization [**72, 74].** High KD values associated with pegmatite bodies suggest hydrothermal modification and guide prioritized geochemical and geophysical follow-up rather than confirming mineralization [**52, 69**].

Fig. 16 highlights linear high-KD alignments along Schist (SU) and Gneiss (BG) boundaries, corresponding to major shear zones and fracture networks [**1**]. The spatial association of KD anomalies with pegmatites and altered lithologies integrates radiometric, structural, and geological observations, emphasizing structurally influenced corridors without assuming confirmed mineralization [**79, 80**]. Areas with dense KD anomalies along these structural corridors are suggested as priority targets for follow-up geochemical sampling, detailed mapping, and ground geophysical surveys. These zones indicate potential pathways for hydrothermal alteration and may be favorable for rare-metal enrichment (Li–Ta–Nb–Sn in pegmatites) or structurally influenced orogenic gold, which requires further field verification [**1, 72, 78].**

ISSN No. 2454-6194 | DOI: 10.51584/IJRIAS |Volume XI Issue VI June 2026

The Field Descriptions of the Rocks In the Study Area

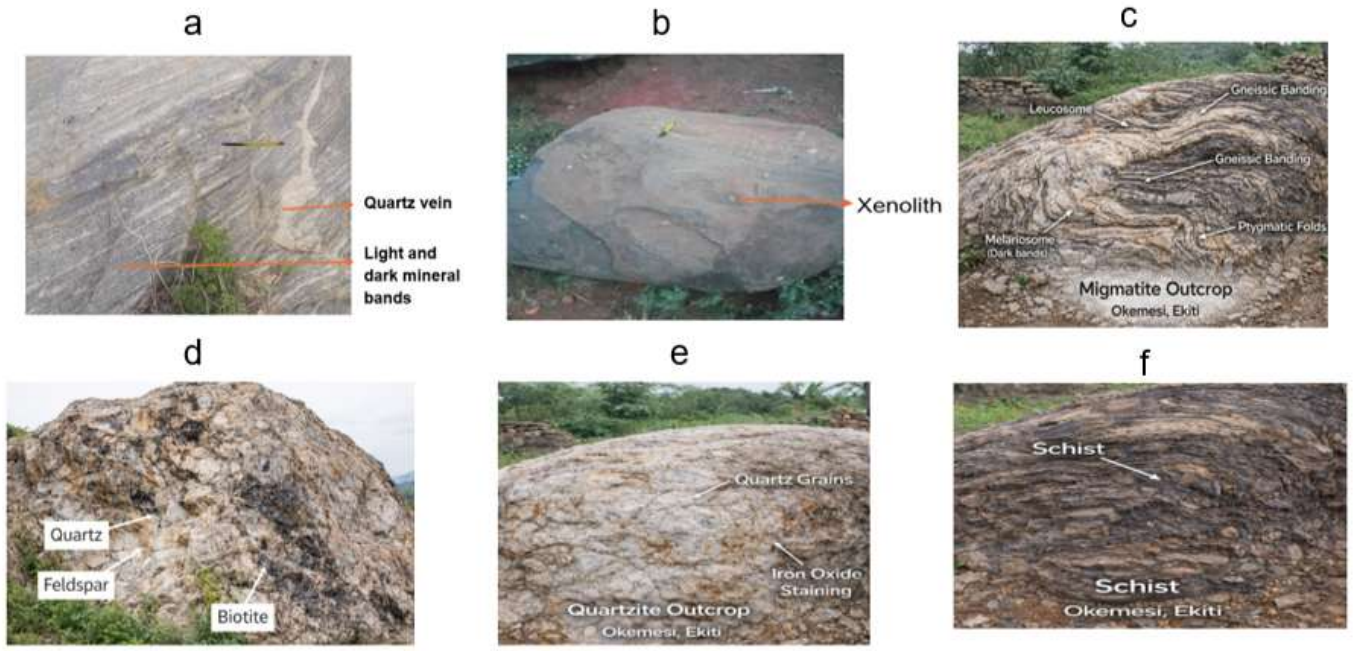

Fig. 17. Field photographs of representative lithological units within the study area at Okemesi, Ekiti, Southwestern Nigeria, showing: **(a)** banded gneiss with well-developed compositional banding and veining; **(b)** charnockite outcrop exhibiting a dark, coarse-grained texture typical of high-grade metamorphic rocks; **(c)** migmatite characterized by alternating leucosome and melanosome layers with prominent ptygmatic folds indicating partial melting; **(d)** pegmatite displaying coarse intergrowths of quartz, feldspar, and biotite typical of late-stage granitic melts; **(e)** quartzite with recrystallized quartz grains and iron-oxide staining along fractures; and **(f)** highly deformed schist showing pronounced foliation and mineral banding, reflecting the complex metamorphic and deformational history of the Precambrian Basement Complex.

The field photograph of the Okemesi outcrop **Fig. 17a** reveals a well-exposed banded gneiss exhibiting pronounced foliation, characterized by alternating light and dark mineral bands [**1,3**]. The lighter bands are dominated by felsic minerals, primarily quartz and feldspar, while the darker bands are enriched in mafic minerals such as biotite and hornblende [**4**]. This compositional layering reflects phase segregation during high-grade regional metamorphism, consistent with the intense deformation associated with the Pan-African orogeny, which has been reported in the southwestern Nigerian Basement Complex [**1, 2**]. The tight to medium layering and subtle variations in band thickness suggest multiple deformation and recrystallization events, corroborating earlier observations by previous workers who identified polyphase metamorphism in the region [**3**]. Minor pegmatitic veins crosscutting the foliation likely represent late-stage intrusions exploiting zones of structural weakness, similar to patterns reported in adjacent basement terrains **[4]**. The overall ductile deformation, foliation orientation, and banding indicate that shear zones and fractures have strongly influenced the regional structural framework [**24].** These gneissic units, therefore, not only record the tectono-metamorphic history of Okemesi but also provide critical control on the localization of hydrothermal fluids and mineralization, bridging gaps in earlier studies that primarily focused on lithology without integrating structural and tectonic implications [**20].** As illustrated in **Fig. 17b**, the charnockite outcrop in Okemesi represents a distinctive member of the Pan-African "Older Granite" suite within the Southwestern Nigerian Basement Complex [**1, 9].** The rock exhibits a dark greenish to greenish-grey hue with a characteristic greasy lustre. Its mineral assemblage comprises quartz, plagioclase, alkali feldspar (commonly perthitic), orthopyroxene (hypersthene), biotite, and hornblende, reflecting ultramafic to intermediate compositions with relatively low silica (<45% SiO_2) and high alumina and iron oxide content [**1, 2].** Texturally, the charnockite is coarse-grained to porphyritic and typically forms low-lying pavements, smooth boulders, or small oval-to-circular hills rising 5–10 m above the surrounding terrain. Structurally, fractures and joints trending NE–SW align with the regional Pan-African tectonic grain, while minor quartz veins and aplite dykes follow similar

ISSN No. 2454-6194 | DOI: 10.51584/IJRIAS |Volume XI Issue VI June 2026

orientations, indicating post-magmatic deformation. In the tropical climate of Okemesi, chemical weathering produces bauxitic clays from feldspar- and pyroxene-rich lithologies, resulting in gently undulating terrain with thick overburden [**1, 3, 4, 6]**. Fresh exposures are locally exploited as dimension stone and high-quality construction aggregate, emphasizing their economic significance. Integrating lithology, structural trends, and weathering patterns provides critical insights into the tectono-metamorphic evolution of the Okemesi basement and highlights potential zones for polymetallic mineralization, complementing findings from aeromagnetic and geochemical investigations [**3, 4].**

The field photograph **Fig. 17c** shows a typical migmatite characterized by alternating light-colored leucosome and dark melanosome layers, forming distinct gneissic banding. The leucosome represents crystallized felsic melt derived from partial melting (anatexis) of the protolith, whereas the melanosome consists of residual mafic minerals such as biotite and hornblende. The presence of ptygmatic folds within the leucocratic veins suggests that the melt was injected and subsequently deformed under ductile conditions during high-temperature metamorphism. Such structures are diagnostic of upper amphibolite to granulite facies metamorphism, typically associated with deep crustal tectonothermal events **[1, 2, 3**]. The irregular folding and segregation of felsic and mafic components reflect melt mobilization and differential competency between layers during deformation. In the context of the Nigerian Basement Complex, migmatites are commonly related to the Pan-African orogeny (~600 Ma), which involved crustal reworking, partial melting, and regional deformation **[1, 2].** The outcrop provides strong evidence of crustal anatexis and syn-metamorphic deformation, indicating that the Okemesi area experienced intense tectono-metamorphic processes consistent with regional basement evolution **[1].**

Fig. 17d depicts a typical coarse-grained pegmatite, characterized by the intergrowth of quartz, feldspar, and biotite. Quartz occurs as milky, interstitial crystals, while feldspar forms large, blocky phenocrysts, often showing albite-twinning. Biotite is present as dark, flaky aggregates, usually concentrated along grain boundaries or cleavage planes. These textures suggest pegmatitic crystallization from a residual granitic melt under slow cooling conditions, allowing large crystals to form **[1, 2].** Such pegmatites are commonly associated with the late stages of crustal differentiation in high-grade metamorphic terrains like the Southwestern Nigerian Basement Complex **[1]. Fig. 17e** displays a well-exposed quartzite outcrop characterized by coarse, interlocking quartz grains. The presence of iron oxide staining along fractures and joints suggests post-metamorphic weathering, likely resulting from oxidation of trace iron-bearing minerals within the quartzite **[1].** The interlocking texture and grain size indicate that the protolith underwent high-grade metamorphism, consistent with the conditions of regional metamorphism typically affecting quartz-rich sandstones [**1, 3].** This outcrop is typical of the quartzite units within the southwestern Nigerian basement complex, reflecting prolonged tectonothermal events that promoted recrystallization and enhanced the hardness of the rock [**1, 2].**

Fig. 17f shows a medium- to high-grade metamorphic rock formed under elevated temperature and pressure conditions. Its most prominent feature is schistosity, characterized by the parallel alignment of platy minerals such as biotite and muscovite, indicative of deformation under differential stress during regional metamorphism [**3, 5].** The wavy, crinkled foliation suggests the rock has experienced multiple deformation phases, consistent with polyphase tectonics. The rock exhibits alternating light and dark layers, reflecting mineral segregation during metamorphism. Darker, flaky layers are likely biotite or chlorite, while lighter, granular layers comprise quartz and feldspar. The characteristic shimmer or "glittery" appearance is due to the reflective surfaces of mica minerals **[1, 2, 5].** Regionally, this outcrop is part of the Schist Belts of Southwestern Nigeria, specifically within the Okemesi area. These rocks originated as sedimentary (shales or mudstones) or volcanic protoliths and were intensely folded and metamorphosed during the Pan-African Orogeny (~600 Ma), reflecting tectonic plate collisions that shaped the West African Basement Complex **[1].**

The reddish-brown surface coloration and fragmented debris indicate a weathering profile, typical of schists, which are prone to mechanical breakdown along foliation planes due to water infiltration and physical erosion **[1, 6, 7].**

ISSN No. 2454-6194 | DOI: 10.51584/IJRIAS |Volume XI Issue VI June 2026

Table 1. The Average Modal (%) Composition Of Minerals In The Slides. This table presents the modal mineralogical composition (%) of representative rock samples from the study area, showing the relative abundance of major and accessory minerals in each lithology. Textures for each sample are also included to provide insights into grain size, fabric, and deformation characteristics, which are important for petrological interpretation and comparative analysis of basement rocks in the Okemesi area.

Slide	Lithology	Sample ID	Qz	Pl	Mc	Or	Bt	Hb	Myr	Cal	Op	Total	Texture
1	Banded Gneiss	ABF-BG	59.50	3.90	1.66	–	38.84	–	–	–	0.65	100	Med–coarse
2	Migmatite	SO-MG	65.36	18.98	12.99	–	2.67	–	–	–	–	100	Fine–med
3	Quartzite	IJ-5A	100	–	–	–	–	–	–	–	–	100	Sugary
4	Migmatite	IDI-3A	80.77	–	–	–	18.27	0.96	–	–	–	100	Med–coarse
5	Migmatite	IJ-5B	60.78	9.80	–	0.98	35.29	–	–	–	2.95	100	Med–coarse
6	Schist	ITW-20A	56.49	3.90	–	3.25	35.71	–	–	–	0.65	100	Med–coarse
7	Charnockite	ITW-2C	72.67	–	–	–	26.16	–	–	–	1.17	100	Coarse
8	Quartzite	OKM-L19	83.33	–	–	–	16.67	–	–	–	–	100	Fine–coarse
9	Granite Gneiss	OKM-L14	62.00	9.80	9.20	–	20.00	–	–	–	–	100	Fine–coarse
10	Quartzite	OKM-5	74.60	–	–	–	–	–	–	–	25.40	100	Sugary
11	Pegmatite	IL-4C	47.00	8.00	32.00	–	13.00	–	–	–	–	100	Coarse
12	Pegmatite	IJ-PM	51.00	23.00	7.00	3.00	13.00	–	3.00	–	–	100	Coarse
13	Charnockite	IK-6	54.00	5.00	7.00	4.00	21.00	3.00	–	–	–	100	Coarse
14	Charnockite	IRO-EK	55.00	4.00	24.00	2.00	15.00	4.00	–	–	–	100	Porphyritic
15	Banded Gneiss	OEEK	51.00	15.00	24.00	4.00	–	5.00	1.23	–	–	100	Gneissic/Porphyritic
16	Migmatite Gneiss	OKI8	58.96	4.48	10.45	2.24	21.64	–	–	–	2.24	100.01	Med–coarse
17	Banded Gneiss	OKM-L1	51.00	–	–	7.41	13.58	–	1.23	–	–	100	Fine–med

ISSN No. 2454-6194 | DOI: 10.51584/IJRIAS |Volume XI Issue VI June 2026

18	Quartzite	ODOW-1	60.00	10.00	–	13.33	–	–	–	–	16.67	100	Sugary

The modal mineralogical composition of the basement rocks in the study area, as summarized in **Table 1**, shows considerable variation across lithologies and samples. Quartz dominates in most samples, ranging from 47% in pegmatite (IL-4C, Slide 11) to 100% in quartzite (IJ-5A, Slide 3), reflecting the silica-rich nature of these basement rocks [**14, 21**]. Plagioclase and alkali feldspars (microcline and orthoclase) are significant in migmatites and granitic rocks, with sample SO-MG (Slide 2) exhibiting 18.98% plagioclase and 12.99% microcline, while IJ-5B (Slide 5) contains 9.8% plagioclase and 0.98% orthoclase, indicating variable magmatic differentiation and partial melting [**17, 22].** Biotite is notably abundant in banded gneiss (ABF-BG, Slide 1; OEEK, Slide 15) and schist (ITW-20A, Slide 6), with proportions up to 38.84%, highlighting the metamorphic influence and foliated textures. Hornblende is mainly present in charnockites (ITW-2C, Slide 7; IK-6, Slide 13) and porphyritic granite (IRO-EK, Slide 14), reflecting crystallization under high-temperature igneous conditions [**43]**. Accessory minerals, including myrmekite and calcite, occur in pegmatite and gneissic samples (IJ-PM, Slide 12; OEEK, Slide 15; OKM-L1, Slide 17), suggesting late-stage magmatic or metasomatic processes **[43, 45].** Minor opaque phases (<2.5%) are recorded in several samples, including ABF-BG (Slide 1) and OKI8 (Slide 16), consistent with the presence of Fe-Ti oxides. Texturally, coarse- to medium-grained textures dominate migmatites, charnockites, and pegmatites, while sugary textures characterize quartzites (IJ-5A, Slide 3; OKM-5, Slide 10) and fine to medium-grained textures are typical of banded gneisses and granites. These mineralogical and textural variations across samples such as FAD-BG, SO-MG, ITW-2C, and OEEK reflect the interplay of igneous crystallization, metamorphism, and deformation in the Okemesi basement complex [**81, 83].**

Table 2: Trace elemental composition (ppm) of rock samples from the study area, showing concentrations of key trace elements for geochemical characterization. The data highlight elemental variations among lithological units and provide insights into petrogenesis, tectonic setting, and mineralization potential.

S/N	Sample	Mo	Cu	Pb	Zn	Ag	Ni	Co	Mn	Au	Th	Sr
1	Aba Francis (Banded Gneiss)	0.05	0.02	0.02	0.2	20	0.1	0.2	2	<0.1	0.1	1
2	Arapate (Charnockite)	0.24	1.03	41.35	4	<20	0.2	20.7	69	<0.1	0.2	11
3	Baba Ori-Oke 8B (Pegmatite)	0.44	9.10	20.19	59.6	203	16.4	24.7	532	<0.1	18.5	122
4	Idao 2 (Quartzite)	0.45	3.79	69.38	41.4	<20	30.6	29.6	322	<0.1	17.8	793
5	Ido-Ile 3A (Schist)	0.45	14.27	58.85	73.8	<20	55.7	29.4	651	<0.1	10.6	610
6	Ido-Ile 3 (Schist)	0.76	0.60	6.11	1.2	37	0.7	77.8	11	<0.1	3.7	29
7	Ijero 4A (Quartzite)	0.40	0.81	4.13	0.8	<20	0.5	40.3	12	<0.1	3.6	30
8	Ijero 4B (Quartzite)	0.35	0.48	3.15	142.3	<20	2.2	30.9	178	<0.1	1	9
9	Ijero 5A (Charnockite)	0.31	0.30	21.48	2.6	<20	0.4	75.4	89	<0.1	2.5	13
10	Ijero 5B (Charnockite)	0.53	0.74	1.29	<0.2	31	20.9	66.4	54	<0.1	0.1	5
11	Iloko L1 (Quartzite)	0.67	0.69	3.9	1.4	<20	1.3	72	6	<0.1	2.7	10
12	Ilokun 4 (Schist)	0.59	0.12	0.86	<0.2	20	0.3	52.2	<2	<0.1	<0.1	<1

Table 2 (continued)

ISSN No. 2454-6194 | DOI: 10.51584/IJRIAS |Volume XI Issue VI June 2026

S/N	Sample	Cd	Sb	Bi	V	Cr	Ba	Zr	Sn	Be	Sc
1	Aba Francis (Banded Gneiss)	0.02	0.02	0.04	1	1	1	0.2	0.1	1	0.1
2	Arapate (Charnockite)	0.05	0.14	0.12	<1	<1	42	11.6	5.5	2	0.6
3	Baba Ori-Oke 8B (Pegmatite)	0.08	0.22	0.20	63	29	638	33.8	4.3	2	10
4	Idao 2 (Quartzite)	0.04	0.04	0.12	29	53	1738	50.5	2.2	5	4.8
5	Ido-Ile 3A (Schist)	0.13	0.19	0.51	42	54	1520	82.8	3.7	5	7.6
6	Ido-Ile 3 (Schist)	0.03	0.26	0.11	2	<1	100	4.2	0.3	<1	0.7
7	Ijero 4A (Quartzite)	<0.02	0.27	0.09	2	<1	77	4.1	0.4	<1	0.5
8	Ijero 4B (Quartzite)	<0.02	0.08	1.3	1	1	29	11.4	131	6	0.7
9	Ijero 5A (Charnockite)	0.05	0.04	0.42	<1	<1	9	3.6	3.3	6	0.4
10	Ijero 5B (Charnockite)	0.03	5.9	<0.04	<1	<1	9	0.4	7.4	2	<0.1
11	Iloko L1 (Quartzite)	<0.02	0.55	0.13	2	2	25	9.6	0.1	<1	0.1
12	Ilokun 4 (Schist)	<0.02	0.09	0.10	<1	<1	2	<0.2	0.2	<1	<0.1

Multivariate statistical analysis of thirty-six geochemical samples from the Okemesi Fold Belt identifies three geochemical populations based on trace element associations (Mo, Cu, Pb, Zn, Ag, Ni, Co, Mn, Au, Th, Sr, Zr, Sn, Cr, Sc) [**42, 43**]. Dataset adequacy is confirmed by Kaiser–Meyer–Olkin (KMO = 0.71) and Bartlett's sphericity test ($p < 0.05$). Cluster I reflects background lithologies with low Cu–Pb–Zn and subdued Co–Ni–Mn contents, consistent with relatively unaltered gneisses and granites [31, 50]. Cluster II represents moderate enrichment along structural zones, potentially influenced by hydrothermal processes associated with shear zones and veins [**81, 78**]. Cluster III shows higher concentrations of Cu, Pb, Zn, Ni, Co, Mn, Cr, Th, and Sn, spatially coinciding with major structural intersections and felsic lithologies, suggesting structurally influenced hydrothermal activity [**80, 82**]. These clusters highlight geochemical variability and potential structural controls, with Cluster III areas being priority targets for further geochemical, petrographic, and geophysical investigations. Overall, the analysis provides a framework for understanding geochemical trends and guides focused exploration within the Okemesi Fold Belt (**Table 2).**

Table 3: Cluster analysis results of geochemical/magnetic data from the study area, showing groupings of samples based on similarity in elemental or magnetic characteristics."

S/n	Sample	Mo	Cu	Pb	Zn	Ag	Ni	Co	Mn	Au	Th	Sr	Zr	Sn	Cr	Sc
1	Aba Francis	0.05	0.02	0.02	0.2	20	0.1	0.2	2	<0.1	0.1	1	0.2	0.1	1	0.1
2	Arapate	0.24	1.03	41.35	4	<20	0.2	20.7	69	<0.1	0.2	11	11.6	5.5	<1	0.6
3	Baba Ori-Oke 8B	0.44	9.1	20.19	59.6	203	16.4	24.7	532	<0.1	18.5	122	33.8	4.3	29	10
4	Idao 2	0.45	3.79	69.38	41.4	<20	30.6	29.6	322	<0.1	17.8	793	50.5	2.2	53	4.8
5	Ido-Ile 3A	0.45	14.27	58.85	73.8	<20	55.7	29.4	651	<0.1	10.6	610	82.8	3.7	54	7.6
6	Ido-Ile 3	0.76	0.6	6.11	1.2	37	0.7	77.8	11	<0.1	3.7	29	4.2	0.3	<1	0.7

ISSN No. 2454-6194 | DOI: 10.51584/IJRIAS |Volume XI Issue VI June 2026

7	Ijero	0.4	0.81	4.13	0.8	<20	0.5	40.3	12	<0.1	3.6	30	4.1	0.4	<1	0.5
8	Ijero Pegmatite	0.35	0.48	3.15	142.3	<20	2.2	30.9	178	<0.1	1	9	11.4	131	1	0.7
9	Ijero 5A	0.31	0.3	21.48	2.6	<20	0.4	75.4	89	<0.1	2.5	13	3.6	3.3	<1	0.4
10	Ijero 5B	0.53	0.74	1.29	<0.2	31	20.9	66.4	54	<0.1	0.1	5	0.4	7.4	<1	<0.1
11	Iloko L1	0.67	0.69	3.9	1.4	<20	1.3	72	6	<0.1	2.7	10	9.6	0.1	2	0.1
12	Ilokun 4	0.59	0.12	0.86	<0.2	20	0.3	52.2	<2	<0.1	<0.1	<1	<0.2	0.2	<1	0.1
13	Ilokun 4c	0.61	2.94	4.13	1.4	<20	0.9	32.5	8	<0.1	1.1	3	6.6	0.5	3	0.3
14	Ikoro 6	1.95	14.73	30.31	56	<20	6.6	49.2	555	<0.1	23.5	278	51.1	4.3	14	9.5
15	Iroro-Ekiti	0.48	0.92	3.1	<0.2	<0.2	0.5	126	2	<0.1	2.8	16	4	0.1	<1	0.4
16	Iroko 2	0.89	0.86	59.73	12.1	48	1.7	25.6	96	<0.1	2	465	53.8	0.4	2	0.9
17	Odo-Owa 1	0.45	1.72	35.11	49.4	23	3.9	25.9	535	<0.1	28.9	255	55.4	3.5	9	5.5
18	Oke-Ila banded gneiss	0.72	1.23	33.01	47.4	34	5.5	29.2	466	<0.1	22.4	336	31.5	4.6	14	8
19	Oke Ila 1	0.7	2.62	22.45	34.7	<20	5.1	23.5	331	<0.1	0.6	79	6.7	2.1	13	6.3
20	Oke-Ila 8	0.27	0.15	19.39	32.5	24	0.4	21.1	314	<0.1	0.3	22	30.2	4.4	2	4
21	Okemesi Road	0.17	0.25	27.72	15.3	<20	0.4	33.8	84	<0.1	0.2	60	10	9.9	<1	1.6
22	Okemesi L1	0.93	3.05	34.46	63.4	<20	2	52.5	565	<0.1	28.5	291	54.3	2.2	6	8.4
23	Okemesi 2	0.44	0.23	1.93	<0.2	<20	3.4	32.5	11	<0.1	1.6	13	5.1	0.2	2	0.3
24	Okemesi 3	0.3	0.51	2.65	0.6	<20	0.6	23.2	14	<0.1	4.6	11	11	0.5	3	1
25	Okemesi 5	0.25	6.45	6.43	5.6	85	4.4	39.6	18	<0.1	8	28	97.6	1.1	16	3.3
26	Okemesi 6	0.44	0.26	1	<0.2	<20	0.7	33.3	2	<0.1	3.5	22	1.6	<0.1	<0.1	0.4
27	Okemesi L9	0.6	3.06	13.47	15.9	69	8.8	26.5	161	<0.1	8.8	85	19.9	1.3	20	3.2
28	Okemesi L14	0.31	1.66	13.14	14.8	<20	6.8	29.7	194	<0.1	6.4	76	30.3	1	11	2.2
29	Okemesi L15	0.83	0.94	15.51	11.3	20	7.7	26.1	150	<0.1	7.1	93	11.5	1	11	2.5
30	Okemesi L19	0.25	0.28	11.56	17.7	40	6.9	43.7	275	<0.1	7.7	146	22	1	9	1.9
31	Osun Epe-Ekiti	0.46	0.95	1.71	<0.2	34	1.1	17.1	25	<0.1	3.3	17	16.8	0.3	<1	0.9
32	Itawure 20A	0.8	1.36	35.08	35.9	<20	1.5	37	364	<0.1	30.8	348	37.9	2.8	4	5.1
33	Itawure 20B	0.35	0.53	0.8	<0.2	<20	0.3	54.5	2	<0.1	2.6	16	1.8	0.1	<1	0.3
34	Itawure 20C	0.57	2	2.17	0.3	<20	1.3	37	6	<0.1	4.6	22	7	0	<1	0.8
35	Soso	0.5	0.29	2.18	0.6	<20	1	38.7	11	<0.1	3.3	12	8.7	0.2	<1	0.7
36	Itawure 20E	0.37	1.03	0.86	<0.2	<20	0.1	30.1	<2	<0.1	2.9	17	2	<0.1	<1	0.4

ISSN No. 2454-6194 | DOI: 10.51584/IJRIAS |Volume XI Issue VI June 2026

The cluster analysis of geochemical and magnetic data from the study area reveals distinct groupings of samples based on elemental and magnetic characteristics, indicating spatial variability in lithology and mineralization potential **[80, 21**]. Samples such as Baba Ori-Oke 8B**,** Idao 2, and Ido-Ile 3A exhibit elevated concentrations of base metals (Cu, Pb, Zn) and trace elements (Ni, Co, Mn), suggesting mineralized zones potentially associated with felsic intrusions or hydrothermal alteration [**14, 79].** In contrast, samples like Aba Francis**,** Ilokun 4**,** and Itawure 20E show low metal concentrations, reflecting background geochemical signatures typical of unaltered basement rocks [**80, 22].** Notably, certain pegmatitic samples, for example Ijero Pegmatite, are characterized by extremely high Zn values and elevated trace metals, consistent with localized enrichment in rare-metal-bearing lithologies. Similarly, high Th, Sr, and Zr concentrations in samples such as Idao 2 and Okemesi L1 indicate the influence of accessory heavy minerals and potential felsic differentiation [**72, 83].** Gold values are generally low across the dataset (<0.1 ppm), suggesting limited auriferous potential in the surveyed sites **[43, 78**]. The clustering highlights areas of geochemical anomalies, with strong correlations between base metal enrichment and trace element concentrations, which can guide further exploration. The spatial distribution of these clusters provides insight into lithological variations, alteration zones, and prospective targets for detailed mineral exploration within the study area [**72, 22]** (**Table 3)**.

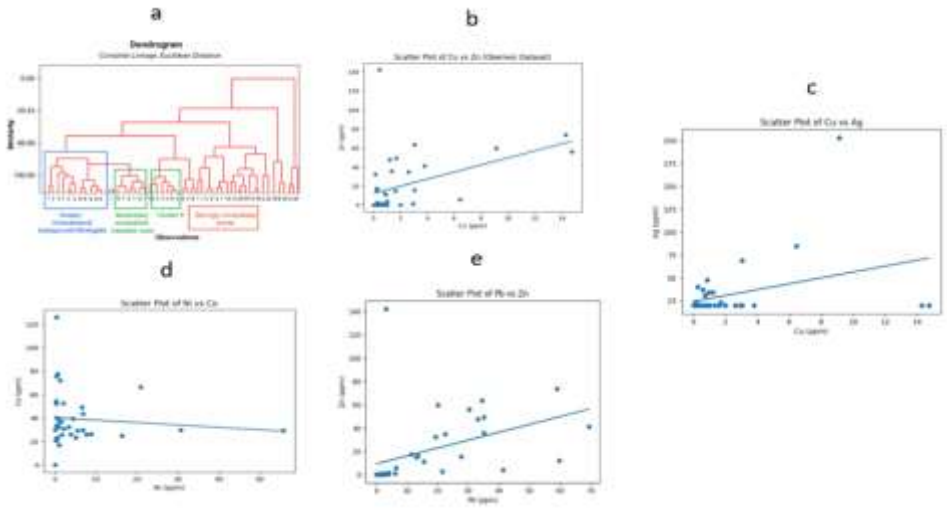

Fig. 18. Geochemical statistical plots for rock samples from Okemesi, Ekiti State, Southwestern Nigeria, showing **(a)** cluster analysis diagram illustrating the grouping of samples based on geochemical similarities and compositional relationships; **(b)** scatter plot of Cu (ppm) versus Zn (ppm) indicating a weak positive correlation ($R^2 \approx 0.19$) and limited geochemical association; **(c)** scatter plot of Cu (ppm) versus Ag (ppm) showing a weak positive correlation ($R^2 \approx 0.12$) that may reflect localized silver enrichment; **(d)** scatter plot of Ni (ppm) against Co (ppm) displaying no significant correlation ($R^2 \approx 0.01$), suggesting independent geochemical behavior; and **(e)** scatter plot of Pb (ppm) versus Zn (ppm) with a weak positive relationship ($R^2 \approx 0.18$), indicating partial base-metal association and heterogeneous mineralization patterns across the study area.

Fig. 18a shows the dendrogram generated using complete linkage and Euclidean distance, which reveals three distinct clusters among the 36 geochemical and magnetic samples from the study area, reflecting variations in mineralization intensity and lithological characteristics **[14, 17].** Cluster I**,** outlined in blue, comprises samples with low similarity in elemental concentrations, representing weakly mineralized zones or background lithologies. These samples exhibit generally low concentrations of base metals (Cu, Pb, Zn) and trace elements (Ni, Co, Mn), indicative of unaltered basement rocks [**80, 83, 84].** Cluster II**,** marked in green, represents a moderately mineralized transition zone. Samples in this group show intermediate levels of base metals and trace elements, suggesting areas influenced by localized hydrothermal alteration or proximity to felsic intrusions. This cluster serves as a geochemical buffer between background lithologies and strongly mineralized zones, highlighting regions of potential exploration interest [**78, 83].** Cluster III**,** highlighted in red, corresponds to strongly mineralized zones. Samples in this cluster display elevated concentrations of Cu, Pb, Zn, Ni, Co, and Mn, along with higher values of Th, Sr, and Zr, which may indicate the presence of accessory heavy minerals and significant hydrothermal enrichment. The distinct separation of this cluster

ISSN No. 2454-6194 | DOI: 10.51584/IJRIAS |Volume XI Issue VI June 2026

reflects high geochemical similarity among mineralized samples, consistent with patterns observed in other basement terrain studies [**22, 43, 81, 83].** The dendrogram effectively delineates geochemical domains within the study area, providing a robust framework for targeted mineral exploration by distinguishing background lithologies, transitional zones, and high-priority mineralized targets. **Fig. 18b** reveals a weak to moderate positive association ($R^2 \approx 0.19$), with several clustered low-background samples and a few distinctly Zn-enriched outliers (e.g., Samples 3, 5, 8, 14, and 22). The dominance of low Cu values (<3 ppm) compared to relatively elevated Zn in some samples suggests preferential Zn enrichment relative to Cu in the study area. Zinc enrichment (e.g., Sample 8: 142.3 ppm Zn with only 0.48 ppm Cu) indicates possible sphalerite-dominated mineralization or selective mobilization of Zn during hydrothermal alteration. In contrast, samples showing comparatively elevated Cu and Zn together (e.g., Samples 5 and 14) may reflect limited polymetallic sulfide association. Such Cu–Zn coupling is characteristic of hydrothermal systems where chalcopyrite ($CuFeS_2$) and sphalerite (ZnS) precipitate under similar physicochemical conditions [**66, 68, 72**]. However, the generally low Cu background suggests that copper mineralization is not strongly developed across most lithologies. The scattered pattern also implies lithological control, particularly within schist and quartzite units, where fluid migration along structural discontinuities may enhance Zn mobility more effectively than Cu. The Cu–Zn relationship suggests localized hydrothermal influence with dominant Zn enrichment and limited copper mineralization, consistent with basement-hosted polymetallic systems [**80, 84]. Fig. 18c** shows a weak positive correlation ($R^2 \approx 0.12$), indicating limited geochemical association between copper and silver within the study area. Although Ag is commonly associated with Cu in hydrothermal sulfide systems, particularly in polymetallic vein deposits, the weak relationship observed here suggests that silver enrichment is not directly controlled by copper mineralization processes. Instead, Ag may be locally concentrated in specific lithologies such as pegmatites or structurally controlled zones. In hydrothermal systems, Ag commonly substitutes into Cu-bearing sulfides such as chalcopyrite and bornite, producing strong positive correlations **[79, 80**]. However, the scattered distribution in the Okemesi dataset implies heterogeneous mineralization, possibly influenced by lithological variability and localized fluid pathways. Such weak element association may reflect multi-stage mineralization or remobilization during metamorphism. Similar observations in basement terrains have been attributed to post-magmatic redistribution processes. **Fig. 18d** shows virtually no correlation ($R^2 \approx 0.01$), indicating independent geochemical behavior. Nickel and cobalt typically display a strong positive correlation in mafic and ultramafic rocks due to their compatible behavior in ferromagnesian minerals such as olivine and pyroxene. A strong relationship usually reflects magmatic control and primary mantle-derived signatures [**68, 72].**

The absence of correlation in the Okemesi samples suggests that Ni and Co are not dominantly controlled by primary magmatic processes. Instead, their distribution may be influenced by lithological heterogeneity, metamorphic redistribution, or weathering effects. In metamorphosed basement complexes, cobalt may partition into sulfides or oxides independently of nickel, especially under varying redox conditions. Such decoupling has been documented in complex basement terrains [**80, 84]**. Therefore, the data imply that mafic affinity is not a dominant geochemical control in the study area. **Fig. 18e** reveals a weak positive correlation ($R^2 \approx 0.18$), indicating partial geochemical association. Lead and zinc commonly occur together in hydrothermal base-metal systems, particularly in galena–sphalerite mineralization. Strong correlations are typically indicative of co-precipitation from the same hydrothermal fluid [**66, 80].** However, the weak association observed in the Okemesi samples suggests heterogeneous mineralization rather than a well-developed, uniform base-metal system. This may reflect structural control, lithological variation, or multi-stage fluid activity. In basement complexes, Pb may be preferentially hosted in feldspar-rich lithologies, while Zn may partition into ferromagnesian or sulfide phases. Such decoupling under metamorphic conditions has been reported in basement terranes [**68, 79].** The weak correlation implies localized enrichment rather than extensive Pb–Zn mineralization, suggesting that mineralization in Okemesi may be structurally controlled and spatially discontinuous.

Table 4: Factor analysis loadings, eigenvalues, and communalities for selected trace elements from the Okemesi Fold Belt. The first three factors (eigenvalues > 1) account for 82.45% of the total variance, indicating strong geochemical control. High loadings define dominant mafic–hydrothermal and structurally controlled element associations.

ISSN No. 2454-6194 | DOI: 10.51584/IJRIAS |Volume XI Issue VI June 2026

Variables	Comp. 1	Comp. 2	Comp. 3	Communalities
Mo	–	–	0.688	0.863
Cu	0.786	–	–	0.865
Pb	–	0.820	–	0.814
Zn	0.776	–	–	0.958
Ag	0.801	–	–	0.841
Ni	0.875	–	–	0.864
Co	–	–	–	0.349
Mn	0.719	–	–	0.959
Th	0.719	0.440	–	0.791
Cr	0.897	–	–	0.940
Eigenvalue	4.66	2.27	1.32	–
VAR (%)	46.587	22.694	13.165	–
CVAR (%)	46.587	69.281	82.446	–

Table 4 presents factor analysis of selected trace elements, extracting three components with eigenvalues greater than 1 (4.66, 2.27, and 1.32), satisfying the Kaiser criterion for retention [**42, 43].** Together, these components explain 82.45% of the total variance, indicating a well-structured multivariate dataset. Component 1 (46.59% variance) is strongly loaded by Cr (0.897), Ni (0.875), Ag (0.801), Cu (0.786), Zn (0.776), Mn (0.719), and Th (0.719), reflecting a dominant geochemical association likely linked to mafic–ultramafic lithologies and possible hydrothermal influence [**76, 78**]. High communalities (>0.84) indicate that most elements are well represented in the extracted components. Component 2 (22.69% variance) is dominated by Pb (0.820) with a moderate contribution from Th (0.440), suggesting a separate geochemical trend potentially associated with felsic lithologies or radiogenic signatures [**78, 81].** Component 3 (13.17% variance) is primarily loaded by Mo (0.688), which may indicate late-stage hydrothermal input or localized element mobility [**82**]. Co shows low communality (0.349), implying limited participation in the main geochemical patterns. Overall, the factor analysis highlights coherent elemental associations and structural–lithological influences on geochemistry, providing a statistically robust framework for further interpretation of geochemical variability in the Okemesi Fold Belt.

Table 5: Correlation coefficient results among measured geochemical and magnetic parameters in the study area. The matrix illustrates the strength and direction of linear relationships between each pair of variables. Positive coefficients indicate a direct relationship, while negative coefficients show an inverse relationship. These correlations help identify potential geochemical associations and controls on mineralization within the basement terrain.

	Mo	Cu	Pb	Zn	Ag	Ni	Co	Mn	Th	Cr
Mo	1									
Cu	0.485	1								

ISSN No. 2454-6194 | DOI: 10.51584/IJRIAS |Volume XI Issue VI June 2026

Pb	0.257	0.420	1							
Zn	0.188	0.379	0.307	1						
Ag	-0.083	0.929	0.087	0.440	1					
Ni	0.029	0.643	0.534	0.374	0.495	1				
Co	0.195	-0.064	-0.201	-0.133	-0.081	-0.092	1			
Mn	0.402	0.634	0.652	0.674	0.354	0.518	-0.184	1		
Th	0.479	0.427	0.503	0.405	0.290	0.219	-0.047	0.774	1	
Cr	-0.021	0.634	0.630	0.234	0.820	0.928	-0.067	0.496	0.260	1

- Correlation is significant at the 0.01 level (1-tailed).
- Correlation is significant at the 0.05 level (1-tailed).

Geochemical correlation patterns reveal associations among trace elements that reflect lithological affinities and potential fluid influence within the Okemesi Fold Belt. Strong positive correlations ($r \geq 0.60$ at the 0.01 significance level) indicate elements that may have co-occurred due to common geochemical processes **[83**]. The Ag–Cu association suggests co-enrichment, potentially related to base-metal sulfide phases such as chalcopyrite or bornite [**53, 84**]. Cr–Ni correlations are consistent with mafic–ultramafic lithologies, particularly amphibolitic belts [**1**]. Positive relationships of Mn with Pb, Zn, and Th may reflect element mobility during metamorphic or hydrothermal processes [**80]**, while moderate Mo–Pb–Cu correlations indicate localized geochemical trends along structural zones [**50]**. These patterns define geochemically coherent domains useful for further investigation, with structurally and lithologically distinct areas serving as key focus zones for detailed geochemical and geophysical studies (**Table 5).**

CONCLUSION AND RECOMMENDATIONS

Conclusion

This study demonstrates that metallic mineralization within the Okemesi Fold Belt is fundamentally controlled by the interplay between basement lithology, Pan-African deformation, and structurally focused hydrothermal fluid flow. The integration of airborne magnetic and radiometric datasets, detailed structural mapping, multivariate geochemical analysis, and petrographic characterization has established a coherent mineralization framework for the study area. Petrographic analysis confirms the mineralogical composition and textural relationships of the host rocks, revealing evidence of deformation-induced recrystallization, hydrothermal alteration, sulfide dissemination, and mineral paragenesis consistent with structurally controlled mineralization. The observed quartz–feldspar recrystallization, sulfide mineral associations, and alteration assemblages corroborate the geochemical and geophysical signatures, thereby strengthening the interpretation of hydrothermal fluid activity along major shear zones and lithological contacts. The spatial convergence of magnetic lineaments, radiometric anomalies, statistically significant element associations, and petrographic alteration features confirms that mineralization in the Okemesi Fold Belt is neither random nor restricted to isolated lithological units. Rather, it is strongly governed by the regional structural architecture of the Precambrian Basement Complex. Shear zones, fault systems, lithological boundaries, and structural intersections acted as primary conduits and depositional traps for mineralizing fluids, resulting in localized enrichment of base metals, rare metals in pegmatitic bodies, and structurally associated gold occurrences. The results underscore the effectiveness of integrating airborne geophysics, geochemistry, petrography, and multivariate statistical analysis in reducing exploration uncertainty and enhancing target delineation within structurally complex crystalline terrains. The identification of structurally controlled mineralized corridors

ISSN No. 2454-6194 | DOI: 10.51584/IJRIAS |Volume XI Issue VI June 2026

emphasizes the economic importance of deformation zones rather than individual lithological units alone. This integrated framework provides a robust and transferable exploration model applicable to basement-hosted mineral systems across southwestern Nigeria and comparable Pan-African terranes.

Recommendations

1. Detailed Ground Geophysical Surveys

High-resolution ground magnetic, induced polarization (IP), electrical resistivity tomography (ERT), and electromagnetic (EM) surveys are recommended across the identified structural corridors. These techniques will refine subsurface geometry, delineate sulfide-rich zones, and detect concealed mineralization beyond surface exposures.

2. Large-Scale Structural and Lithological Mapping

Detailed structural mapping at scales of 1:10,000 or finer should be undertaken to better constrain shear zone kinematics, deformation intensity, structural intersections, and hydrothermal alteration footprints. Such mapping will enhance understanding of fluid pathways and mineral trapping mechanisms.

3. Systematic Trenching and Core Drilling

Targeted trenching and diamond drilling programs within priority anomalous zones are essential to validate subsurface continuity, establish grade distribution, and evaluate economic viability. Drilling will also provide fresh samples for advanced mineralogical and geochemical studies.

4. Advanced Geochemical and Isotopic Studies

Although petrography has been completed, further refinement through fluid inclusion microthermometry, stable isotope geochemistry, and detailed mineral chemistry is recommended to constrain fluid sources, temperature–pressure conditions, and the timing of mineralization relative to deformation events.

5. Three-Dimensional Integrated Geological Modeling

Development of a 3D structural–geophysical–geochemical model incorporating petrographic constraints will enhance predictive targeting and provide a comprehensive decision-support framework for future exploration campaigns.

6. Regional Application of the Exploration Model

The integrated exploration methodology developed in this study should be extended to other segments of the Nigerian Basement Complex and analogous Pan-African terranes across West Africa to test its regional applicability and scalability.

Declaration of competing interests

Ethical Approval

This study did not involve human participants, animals, or any form of clinical or ethical experimentation. All data were obtained from field observations, rock sampling, and laboratory analyses**,** which pose no risk to living beings or personal privacy. Therefore, formal ethical approval was not required**.**

Declaration of generative AI and AI-assisted technologies in the manuscript preparation process

During the preparation of this work, the authors used ChatGPT (GPT-5-mini) to assist with language editing and content organization. After using this tool, the authors reviewed, revised, and verified all content to ensure accuracy, originality, and authenticity, and take full responsibility for the content of the published article.

Consent to Participate

As no human participants were involved in this research, obtaining consent for participation was not applicable**.** All research activities adhered to standard field and laboratory protocols without the involvement of people.

Consent to Publish

This study does not include any personal, sensitive, or identifiable information. Consequently, consent to publish was not applicable. All data presented are scientific observations and analyses, fully anonymized, and pose no ethical concerns.

Funding

This research received no specific grant from any funding agency in the public, commercial, or not-for-profit sectors.

Conflicts of Interest

The authors declare that they have no known competing financial interests or personal relationships that could have appeared to influence the work reported in this paper.

Availability of Data and Materials

The datasets used and analyzed during this study are available from the corresponding author upon reasonable request.

Author Contributions

Adebisi Matthew Iwabi: Conceptualization, geophysical data processing, interpretation, and manuscript drafting.

Ayodele Samuel Olusiji: Supervision, geological interpretation, and manuscript review and editing.

Olususi Joseph Ige: Data acquisition, geological mapping, and geochemical interpretation. All authors reviewed and approved the final version of the manuscript.

ACKNOWLEDGEMENTS

The authors sincerely thank God for His guidance, wisdom, and provision throughout the course of this research.

REFERENCES

1. **Rahaman, 1988** M.A. Rahaman Recent advances in the study of the basement complex of Nigeria In: Precambrian Geology of Nigeria, Geological Survey of Nigeria (1988), pp. 11–43. Available at: https://www.sciepub.com/reference/318092
2. **Ajibade and Wright, 1989** A.C. Ajibade, J.B. Wright The Togo–Benin–Nigeria shield: Evidence of crustal aggregation in the Pan-African belt Tectonophysics, 165 (1989), pp. 125–129, https://doi.org/10.1016/0040-1951(89)90041-3
3. **Omosanya et al., 2009** K. Omosanya, S.O. Ariyo, U. Kaigama, G.O. Mosuro, T.A. Laniyan An outcrop evidence for polycyclic orogenies in the basement complex of southwestern Nigeria J. Geogr. Geol., 7(3) (2009), pp. 24–34. Available at: https://ccsenet.org/journal/index.php/jgg/article/view/49753
4. **Osita et al., 2025** L.J. Osita, A. Mallam, N.N. Abdulsalam, G.J. Nzeghi Integrated gravity and magnetic derivative modelling for structural control of gold mineralization in

north-central Nigeria Asian J. Geol. Res., 8(3) (2025), pp. 376–391. Available at: https://journalajoger.com/index.php/AJOGER/article/view/205

5. **Obasi and Oluwatoyin, 2020** R.A. Obasi, O.A. Oluwatoyin The migmatite and gneisses in the basement complex of southwestern Nigeria: A re-appraisal of their structural, mineralogical, and geochemical diversity IJRDO J. Appl. Sci., 6(8) (2020), pp. 1–17. Available at: https://www.ijrdo.org/index.php/as/article/view/3817
6. **Talabi et al., 2018** A.O. Talabi, A.O. Oyinloye, O.A. Olaolorun, R.A. Obasi, A.B. Eluwole, O.F. Adebayo, O.L. Ademilua Petrography and geochemistry of Orin-Ekiti basement rocks, southwestern Nigeria: Implications on bauxitization Am. J. Appl. Sci., 15(4) (2018), pp. 230–239. https://doi.org/10.3844/ajassp.2018.230.239
7. **Oyinloye, 2011** A.O. Oyinloye Geochemistry and geotectonic setting of the Precambrian basement complex rocks of southwestern Nigeria Earth Environ. Sci., (IntechOpen) (2011). https://doi.org/10.5772/26990
8. **Akinduko et al., 2022** O.K. Akinduko, K. Salako, D.U. Alhassan, J. Lawrence, A. Alkali, B. Aliyu, L. Damidami Aeromagnetic and aeroradiometric prospecting for potential gold mineralisation over Ilesha and its environs, southwestern Nigeria Asian J. Geol. Res., 5(3) (2022), pp. 199–214. Available at: https://journalajoger.com/index.php/AJOGER/article/view/124
9. **Ogunyele et al., 2017** A. Ogunyele, O. Adegbuyi, M. Odindu, T. Erinfolami Geochemical characteristics and petrogenesis of basement rocks in Idoani area, Ondo State, southwestern Nigeria Int. J. Adv. Geosci., 5(2) (2017), pp. 102–108. https://doi.org/10.14419/ijag.v5i2.8377
10. **Arogundade et al., 2022** A.B. Arogundade, M.O. Awoyemi, O.D. Ajama, S.C. Falade, O.S. Hammed, O.A. Dasho, C.A. Adenika Integrated aeromagnetic and airborne radiometric data for mapping potential areas of mineralisation deposits in parts of Zamfara, north-west Nigeria Pure Appl. Geophys., 179(1) (2022), pp. 351–369. https://doi.org/10.1007/s00024-021-02913-w
11. **Ojo et al., 2020** A. Ojo, M. Adeloye, I. Egbedele, F. Akinwande Magnetic rocks distribution and depth to basement analysis on an old quarry site, Abeokuta, SW Nigeria Iran. J. Earth Sci., 12(3) (2020), pp. 176–183. Available at: https://oiccpress.com/ijes/article/view/5669
12. **Ademila et al., 2018** O. Ademila, A.S. Akingboye, A.I. Ojamomi Radiometric survey in the geological mapping of parts of the basement complex area of Nigeria Vietnam J. Earth Sci., 40(3) (2018). https://doi.org/10.15625/0866-7187/40/3/12619
13. **Abubakar et al., 2024** F. Abubakar, J.O. Alao, A.J. Ogah, S. Uche, et al. Evaluation of gold mineralisation potential using AHP systems and weighted overlay analysis Sci. Rep., 14 (2024), Article 21263. https://doi.org/10.1038/s41598-024-70957-8
14. **Rollinson, 1993** H.R. Rollinson Using geochemical data: Evaluation, presentation, interpretation Longman Sci. & Tech./Wiley, 1993. https://doi.org/10.4324/9781315845548
15. **Kabata Pendias, 2011** A. Kabata Pendias Trace elements in soils and plants, 4th ed. Boca Raton, FL: CRC Press / Taylor & Francis Group, 2011. https://www.taylorfrancis.com/books/ mono/10.1201/ b10158/trace-elements-soils-plants-alina-kabata-pendias
16. **Akinlalu et al., 2018** A.A. Akinlalu, A.O. Adelusi, G.M. Olayanju, K.A.N. Adiat, G.O. Omosuyi, A.Y.B. Anifowose, B.E. Akeredolu Aeromagnetic mapping of basement structures and mineralization characterization of Ilesa Schist Belt, southwestern Nigeria J. Afr. Earth Sci., 138 (2018), pp. 383–391. Available at: https://sdiopr.s3.ap-south-1.amazonaws.com/2024/Apr/13-Apr-24/2024 JGEESI 115647/Ms_JGEESI_115647.pdf
17. **Rose et al., 1979** A.W. Rose, H.E. Hawkes, J.S. Webb Geochemistry in mineral exploration London/New York: Academic Press, 1979. xvii + 657 pp. Available at: https://catalogue.nla.gov.au/catalog/2905023
18. **Salawu et al., 2023** N.B. Salawu, K.O. Omosanya, A.B. Eluwole, J. Ajadi, L.S. Adebiyi Structurally-controlled gold mineralization in the Southern Zuru Schist Belt, NW Nigeria: Application of remote sensing and geophysical methods J. Appl. Geophys., 211 (2023), Article 104969. https://doi.org/10.1016/j.jappgeo.2023.104969
19. **Ogunyele et al., 2020** A.C. Ogunyele, O.A. Oluwajana, I.Q. Ehinola, B.E. Ameh, T.A. Salaudeen Petrochemistry and petrogenesis of the Precambrian Basement Complex rocks around Akungba Akoko,

southwestern Nigeria Mater. Geoenviron., 66(3) (2020), pp. 173–183. https://doi.org/10.2478/rmzmag-2019-0036

20. **Akeredolu et al., 2022** B.E. Akeredolu, K.A. Adiat, A.A. Akinlalu, G.M. Olayanju Relationship between morpho-structural features and borehole yield in Ilesha Schist Belt, southwestern Nigeria: Results from geophysical studies Earth Sci., 11(1) (2022), pp. 16–28. https://doi.org/10.11648/j.earth.20221101.13
21. **Adetunla et al., 2024** F.R. Adetunla, A.G. Isah, I.O. Oladapo, O.A. Akinbiyi, A.S. Oji Soil survey and lithogeochemical techniques in mineral exploration Int. J. Res. Innov. Appl. Sci. (IJRIAS), 9(3) (2024), pp. 390–405. Available at: https://rsisinternational.org/journals/ijrias/DigitalLibrary/volume-9-issue-3/390-405.pdf
22. **Govett, 1983** G.J.S. Govett Rock geochemistry in mineral exploration In: Handbook of Exploration Geochemistry, Volume 3. Elsevier Scientific Publishing Company, 1983. Available at: https://api.pageplace.de/preview/DT0400.9781483289700_A23884968/preview-9781483289700_A23884968.pdf
23. **Obaje, 2009** N.G. Obaje Geology and mineral resources of Nigeria Berlin: Springer, 2009. Lecture Notes in Earth Sciences, vol. 120. https://doi.org/10.1007/978-3-540-92685-6
24. **Ayodele and Odeyemi, 2010** O.S. Ayodele, I.B. Odeyemi Analysis of the lineaments extracted from LANDSAT TM image of the area around Okemesi, south-western Nigeria Indian J. Sci. Technol., 4(1) (2010), pp. 31–36. https://doi.org/10.17485/ijst/2011/v4i1.17
25. **Nigerian Geological Survey Agency (NGSA), 2006** Nigerian Geological Survey Agency – NGSA Geophysical mapping of Nigeria: Airborne radiometric and magnetic survey data, 2006. Available at: https://ngsa.gov.ng
26. **Macmillan and Maus, 2005** S. Macmillan, S. Maus International Geomagnetic Reference Field—the tenth generation Earth Planets Space, 57(12) (2005), pp. 1135–1140. https://doi.org/10.1186/BF03351896
27. **Oyawoye, 1972** M.O. Oyawoye The basement complex of Nigeria In: T.F.J. Dessauvagie, A.J. Whiteman, editors, African Geology. Ibadan: University of Ibadan Press, 1972, pp. 66–102. Available at: https://www.worldcat.org/title/6791305
28. **Rahaman, 1976** M.A. Rahaman Review of the basement geology of southwestern Nigeria In: C.A. Kogbe, editor, Geology of Nigeria. Lagos: Elizabethan Publishing Company, 1976, pp. 41–58. Available at: https://www.scirp.org/reference/referencespapers?referenceid=2240797
29. **Ominigbo, 2022** O.E. Ominigbo Evolution of the Nigerian Basement Complex: Current status and suggestions for future research J. Min. Geol., 58(1) (2022), pp. 229–236. Available at: https://www.researchgate.net/publication/361037052_Evolution_of_the_Nigerian_Basement_Complex_Current_Status_and_Suggestions_for_Future_Research
30. **Lukman et al., 2024** L.M. Lukman, T. Najime, P.O. Ogunleye, S. Magaji, N.K. Caleb Geology and geochemical characterization of basement rocks around Burumburum area, North Central Basement Complex, Nigeria Earth Sci., 13(1) (2024), pp. 14–38. https://doi.org/10.11648/j.earth.20241301.13
31. **Elueze, 1982** A.A. Elueze Geochemistry of the Ilesha granite gneiss in the basement complex of southwestern Nigeria Precambrian Res., 19(2) (1982), pp. 167–177. https://linkinghub.elsevier.com/retrieve/pii/0301926882900572
32. **Bamisaiye and Ajala, 2021** O.A. Bamisaiye, P.T. Ajala Pan African Nappe system: Evidence of thrust structures from Okemesi, southwestern Nigeria Heliyon, 7(6) (2021), e07174. https://www.sciencedirect.com/science/article/pii/S2405844021012779
33. **Adeoti and Okonkwo, 2016** B. Adeoti, C.T. Okonkwo Structural geology of the basement complex rocks in Iwaraja area, southwestern Nigeria Int. Lett. Nat. Sci., 58 (2016), pp. 16–28. https://www.academicoa.com/ILNS.58.16.pdf
34. **Adeleye et al., 2020** D.R. Adeleye, O.O. Alabi, F. Ogunwale Structural controls on metallic mineralization in the Okemesi Fold Belt, Southwestern Nigeria Ore Geol. Rev., 120 (2020), 103379. https://doi.org/10.1016/j.oregeorev.2020.103379
35. **Adeoti and Okonkwo, 2017** B. Adeoti, C.T. Okonkwo Structural evolution of Iwaraja shear zone, southwestern Nigeria J. Afr. Earth Sci., 131 (2017), pp. 117–127. https://www.sciencedirect.com/science/article/abs/pii/S1464343X17301516

36. **Faruwa et al., 2021** A.R. Faruwa, W. Qian, O.S. Obafunmilayo, B.B. Daramola, C. Dusabemariya, U.I. Markus Airborne magnetic and radiometric mapping for litho-structural settings and its significance for bitumen mineralization over the Agbabu bitumen belt, southwestern Nigeria J. Afr. Earth Sci., 180 (2021), 104222. https://doi.org/10.1016/j.jafrearsci.2021.104222
37. **Blakely and Simpson, 1986** R.J. Blakely, R.W. Simpson Approximating edges of source bodies from magnetic or gravity anomalies Geophysics, 51(7) (1986), pp. 1494–1498. https://doi.org/10.1190/1.1442197
38. **Stewart, 2019** I.C.F. Stewart A simple approximation for low latitude magnetic reduction to the pole J. Appl. Geophys., 166 (2019), pp. 57–67. https://doi.org/10.1016/j.jappgeo.2019.04.021
39. **Li and Oldenburg, 1998** Y. Li, D.W. Oldenburg Separation of regional and residual magnetic field data Geophysics, 63(2) (1998), pp. 431–439. https://doi.org/10.1190/1.1887567
40. **Reid et al., 1990** A.B. Reid, J.M. Allsop, H. Granser, A.J. Millett, I.W. Somerton Magnetic interpretation in three dimensions using Euler deconvolution Geophysics, 55(1) (1990), pp. 80–91. https://doi.org/10.1190/1.1442774
41. **Verduzco et al., 2004** B. Verduzco, J.D. Fairhead, C.M. Green, C. MacKenzie New insights into magnetic derivatives for structural mapping Lead. Edge, 23(2) (2004), pp. 116–119. https://doi.org/10.1190/1.1651454
42. **Van Loon and Barefoot, 1989** J.C. Van Loon, R.R. Barefoot Analytical methods for geochemical exploration Academic Press (1989). https://doi.org/10.1016/C2009-0-21709-0
43. **Chao, 1984** T.T. Chao Use of partial dissolution techniques in geochemical exploration J. Geochem. Explor., 20(2) (1984), pp. 101–135. https://doi.org/10.1016/0375-6742(84)90078-5
44. **Ilugbo et al., 2020** S.O. Ilugbo, H.O. Edunjobi, O.E. Adewoye, T.O. Alabi, A.I. Aladeboyeje, O.O. Olutomilola, D.T. Owolabi Structural analysis using integrated aeromagnetic data and Landsat imagery in a basement complex terrain, Southwestern Nigeria Asian J. Geol. Res., 3(2) (2020), pp. 78–94. https://journalajoger.com/index.php/AJOGER/article/view/105
45. **Tawey et al., 2020** M.D. Tawey, D.U. Alhassan, A.A. Adetona, K.A. Salako, A.A. Rafiu, E.E. Udensi Application of aeromagnetic data to assess the structures and solid mineral potentials in part of North Central Nigeria J. Geogr. Environ. Earth Sci. Int., 24(5) (2020), pp. 11–29. https://doi.org/10.9734/jgeesi/2020/v24i530223
46. **Ekwok et al., 2024** S.E. Ekwok, A.M. Eldosouky, E.A. Thompson, R.A. Ojong, A.M. George, S.S. Alarifi, et al. Mapping of geological structures and sediment thickness from analysis of aeromagnetic data over the Obudu Basement Complex of Nigeria J. Geophys. Eng., 21(2) (2024), pp. 413–425. https://doi.org/10.1093/jge/gxae012
47. **Muhammad et al., 2025** S.B. Muhammad, S.A. Ogunsina, N.M. Muztaza Geophysical prospecting for mineral potential zones in Zamfara and environs, Northern Nigeria basement complex UMYU Scientifica, 4(2) (2025), pp. 115–121. https://doi.org/10.56919/usci.2542.014
48. **Olawuyi, 2020** A.K. Olawuyi Application of aeromagnetic data and pseudo gravity transforms in the analysis of subsurface structures and mineralization potential, Osi NE, Southwestern Nigeria Ilorin J. Sci., 7(2) (2020), pp. 208–226. https://doi.org/10.54908/iljs.2020.07.02.006
49. **Taiwo and Damidami, 2025** A. Taiwo, L. Damidami Aero-magnetic and aero-radiometric prospecting for potential gold mineralisation over Ilesha and its environs, Southwest, Nigeria Asian J. Geol. Res., 2025. https://journalajoger.com/index.php/AJOGER/article/view/124
50. **Ogunkoya and Alasi, 2025** C.O. Ogunkoya, T.K. Alasi Integrating aeromagnetic data for subsurface characterization in the Ilesha Schist Belt Geol. Behav., 2025. https://geologicalbehavior.com/gbr-02-2025-62-68/
51. **Ohaegbuchu et al., 2024** H.E. Ohaegbuchu, O.C. Dinneya, E.U. Nwokoma, S.I. Uzoaru, Y.A. Musa Unconstrained 3D inversion of airborne magnetic data for mineral targeting in the Southwestern Nigerian Basement Complex Nig. J. Phys., 34(3) (2024), pp. 135–150. https://njp.nipngr.org/index.php/njp/article/view/425
52. **Crawford et al., 2024** A.F. Crawford, N. Thébaud, et al. Structural and rheological controls on hydrothermal fluid flux within orogenic gold systems—insights from the Oberon deposit (Granites-Tanami Orogen) Econ. Geol., 119(8) (2024), pp. 1809–1832. https://doi.org/10.5382/econgeo.5116

53. **Olayinka et al., 2019** A.I. Olayinka, O.E. Fashola, E.A. Ayolabi, A.I. Olayinka Structural mapping and gold mineralisation potential evaluation from airborne time domain electromagnetic (TDEM) data of Ilesha Schist Belt, southwestern Nigeria Explor. Geophys., 53(3) (2019), pp. 237–254. https://doi.org/10.1080/08123985.2021.1922275
54. **Golani, 2021** P.R. Golani Assessment of ore deposit settings, structures, and proximity indicator minerals in geological exploration Springer Mineral., 2021. https://doi.org/10.1007/978-3-030-65125-1
55. **Olatunji et al., 2021** S. Olatunji, et al. Integration of remote sensing and geophysical methods for structural and lithological mapping in Precambrian basement rocks, Northern Nigeria J. Fundam. Appl. Sci., 14(1) (2021), pp. 161–180. https://doi.org/10.4314/jfas.v14i1.9
56. **Adepoju, 2022** M.O. Adepoju Structural control of ore mineralization in the southeastern margin of the Western Nigeria Basement Int. J. Geosci., 13 (2022), pp. 547–556. https://doi.org/10.4236/ijg.2022.137029
57. **Nnaemeka et al., 2021** E.K. Nnaemeka, D.N. Obiora, J.C. Ibuot Structural interpretation and depth to the magnetic basement using aeromagnetic data of Nkalagu and Abakaliki areas, Southeastern Nigeria Int. J. Earth Sci. Geophys., 7(2) (2021), 054. https://vibgyorpublishers.org/content/ijesg/fulltext.php?aid=ijesg7_054
58. **International Atomic Energy Agency (IAEA), 2003** International Atomic Energy Agency (IAEA) Guidelines for radioelement mapping using gamma-ray spectrometry data IAEA-TECDOC-1363, Vienna, Austria (2003). https://www-pub.iaea.org/mtcd/publications/pdf/te_1363_web.pdf
59. **Ahl et al., 2013** A. Ahl, K. Motschka, P. Slapansky Precipitation correction of airborne gamma-ray spectrometry data using monitoring profiles: methodology and case study Explor. Geophys., 45(1) (2013), pp. 8–15. https://doi.org/10.1071/EG12075
60. **Seltmann et al., 2014** R. Seltmann, T.M. Porter, F. Pirajno Geodynamics and metallogeny of the Central Eurasian porphyry and related epithermal mineral systems: A review J. Asian Earth Sci., 79 (2014), pp. 810–841. https://doi.org/10.1016/j.jseaes.2013.03.030
61. **Onyejiuwaka and Nwokeabia, 2020** I.S. Onyejiuwaka, C.N. Nwokeabia Application of airborne radiometric method in geologic mapping of Malufashi area and environs, Northwestern Nigeria Int. J. Adv. Geosci., 8(2) (2020), pp. 179–185. https://doi.org/10.14419/ijag.v8i2.31071 https://sciencepubco.com/index.php/IJAG/article/view/31071
62. **Richards, 2011** J.P. Richards Magmatic to hydrothermal metal fluxes in convergent and collided margins Ore Geol. Rev., 40 (2011), pp. 1–26. https://doi.org/10.1016/j.oregeorev.2011.05.006
63. **O'Reilly and Corey, 1988** G.A. O'Reilly, M.C. Corey The role of airborne gamma ray spectrometry in bedrock mapping and mineral exploration: case studies from granitic rocks within the Meguma Zone, Nova Scotia Atlant. Geosci., 24(1) (1988). https://doi.org/10.4138/1639
64. **Cooke and Simmons, 2000** D.R. Cooke, S.F. Simmons Characteristics and genesis of epithermal gold deposits In: Gold in 2000: Proceedings of the Seventh International Symposium on Geology of Gold Deposits, GeoScienceWorld Books, 2000, pp. 89–115. https://doi.org/10.5382/Rev.13.06
65. **Robb, 2005** L.J. Robb Introduction to ore forming processes, Blackwell Publishing, 2005. https://openlibrary.org/books/OL7621945M/Introduction_to_Ore-Forming_Processes
66. **Assran et al., 2025** A.S.M. Assran, M.M. El-Sayed, A.S. El-Zehery, M.M. Youssef Delineating the uranium anomalous zones using remote sensing and radiometric data: a case study from Gabal Umm Tinassib area, North Eastern Desert, Egypt J. Umm Al-Qura Univ. Appl. Sci., 2025. https://doi.org/10.1007/s43994-024-00158-6 https://link.springer.com/article/10.1007/s43994-024-00158-6
67. **Nabighian et al., 2005** M.N. Nabighian, V.J.S. Grauch, R.O. Hansen, T.R. LaFehr, Y. Li, J.W. Peirce, J.D. Phillips, M.E. Ruder The historical development of the magnetic method in exploration Geophysics, 70(6) (2005), pp. 33ND–61ND. https://doi.org/10.1190/1.2133784
68. **Berger and Henley, 2011** B.R. Berger, R.W. Henley Magmatic vapor expansion and the formation of high sulfidation gold deposits: Structural controls on hydrothermal alteration and ore mineralization Ore Geol. Rev., 39(1–2) (2011), pp. 75–90. https://doi.org/10.1016/j.oregeorev.2010.11.004
69. **Odeyemi, 1982** I. Odeyemi A review of the orogenic events in the Precambrian basement of Nigeria, West Africa Geol. Rundsch., 70 (1982), pp. 897–909. https://doi.org/10.1007/BF01820170

70. **Thurston and Smith, 1997** J.B. Thurston, R.S. Smith Automatic conversion of magnetic data to depth, dip, and susceptibility contrast using the SPITM method Geophysics, 62(3) (1997), pp. 807–813. https://doi.org/10.1190/1.1444190
71. **Salawu et al., 2021** N.B. Salawu, S.S. Dada, M.M. Orosun, L.S. Adebiyi, O. Fawale Influence of Pan-African tectonics on older Precambrian basement structural fabrics as revealed from the interpretation of aeromagnetic and remote sensing data of Ikole/Kabba region, southwestern Nigeria J. Afr. Earth Sci., 179 (2021), 104189. https://doi.org/10.1016/j.jafrearsci.2021.104189
72. **Melcher et al., 2013** F. Melcher, T. Graupner, H.E. Gäbler, M. Sitnikova, F. Henjes Kunst, T. Oberthür Tantalum–(niobium–tin) mineralisation in African pegmatites and rare metal granites: constraints from Ta–Nb oxide mineralogy, geochemistry and U–Pb geochronology Ore Geol. Rev., 64 (2013), pp. 667–719. https://doi.org/10.1016/j.oregeorev.2013.09.003
73. **Amigun et al., 2022** J.O. Amigun, S.O. Sanusi, L. Audu Geophysical characterization of rare earth element and gemstone mineralisation in the Ijero Aramoko pegmatite field, southwestern Nigeria J. Afr. Earth Sci., 188 (2022), 104494. https://doi.org/10.1016/j.jafrearsci.2022.104494
74. **Černý et al., 2005** P. Černý, T.S. Ercit, D. London The classification of granitic pegmatites revisited Can. Mineral, 43(6) (2005), pp. 2005–2026. https://doi.org/10.2113/gscanmin.43.6.2005
75. **Ologe et al., 2025** O. Ologe, A.M. Moyi, F. Sanusi, U.H. Tsafe, S. Umar Interpretation of airborne radiometric data of a typical Basement Complex, Northwest Nigeria ARID ZONE J. Eng. Technol. Environ., 21(1) (2025), pp. 294–302. https://www.azojete.com.ng/index.php/azojete/article/view/1032
76. **Woakes et al., 1987** M. Woakes, M.A. Rahaman, A.C. Ajibade Some metallogenetic features of the Nigerian Basement J. Afr. Earth Sci., 6(5) (1987), pp. 655–664. https://doi.org/10.1016/0899-5362(87)90004-2
77. **Bamigboye et al., 2022** O.S. Bamigboye, T.E. Bamidele, A.D. Adedoyin, T.A. Issa, O.A. Omorinoye Shear sense analyses of Basement Complex rocks in parts of SW Nigeria Int. J. Earth Sci. Knowl. Appl., 2022. https://www.ijeska.com/index.php/ijeska/article/view/151
78. **Reimann and Filzmoser, 2000** C. Reimann, P. Filzmoser Normal and lognormal data distribution in geochemistry: death of a myth. Consequences for the statistical treatment of geochemical and environmental data Environ. Geol., 39(9) (2000), pp. 1001–1014. https://link.springer.com/article/10.1007/s002549900081
79. **Talapatra, 2020** A.K. Talapatra Geochemical exploration and modelling of concealed mineral deposits Springer Int. Publ., 2020. https://link.springer.com/content/pdf/10.1007/978-3-030-48756-0.pdf
80. **Boyle, 1979** R.W. Boyle The geochemistry of gold and its deposits (together with a chapter on geochemical prospecting for the element) Geol. Surv. Canada Bull. 280 (1979), 584 pp. https://publications.gc.ca/collections/collection_2016/rncan-nrcan/M42-280-1-eng.pdf
81. **Fersman et al., 1952** A.Ye. Fersman, S.A. Borovik, G.V. Gorshkov, S.D. Popov, A.F. Sosedko, L. Hartsock, A.P. Pierce Geochemical and mineralogical methods of prospecting for mineral deposits U.S. Geol. Surv. Circ. 127, U.S. Government Printing Office; 1952. https://pubs.usgs.gov/publication/cir127
82. **Taylor and McLennan, 1985** S.R. Taylor, S.M. McLennan The continental crust: its composition and evolution Blackwell Sci. Publ., 1985. https://commons.library.stonybrook.edu/geo-articles/12/
83. **Zhang et al., 2005** C. Zhang, F.T. Manheim, J. Hinde, J.N. Grossman Statistical characterization of a large geochemical database and the effect of sample size Appl. Geochem., 20(10) (2005), pp. 1857–1874. https://www.usgs.gov/publications/statistical-characterization-a-large-geochemical-database-and-effect-sample-size
84. **Asubiojo et al., 2022** M.T. Asubiojo, K.O. Olomo, O.K. Olaleye, J.B. Olatunbosun Characterisation of gold-associated base metals in Itagunmodi, Ilesha Schist Belts, Nigeria, to ascertain their ore body formation trends Earth Sci. Pak., 6(1) (2022), pp. 36–42. https://earthsciencespakistan.com/esp-01-2022-36-42/